2019

Master's thesis

Neural Representation of 3D Orientation of Objects: an fMRI study

1217002 Thanaphop Threethipthikoon

Advisor Assoc. Prof. Hiroaki Shigemasu

September 2019

Informatics Course

Graduate School of Engineering, Kochi University of Technology

Abstract

Neural Representation of 3D Orientation of Objects: an fMRI study

Thanaphop Threethipthikoon

The representation of three-dimensional (3D) orientation is a fundamental feature of human vision which has been broadly studied in recent years. The cortical representation of stereoscopic 3D surface was investigated in the previous study, and the result showed that some regions of interest (ROI) in intraparietal sulcus (IPS) had a tendency for 3D shape orientation classification. Since it is well known that IPS area is involved in vision for action, we adopted different stimuli that were expected to produce a better classification to verify that the action related graspable feature has effected on objects orientation perception. In this study, the 3D objects related to action were used for orientation classification with two different types of orientation, (1) slant-tilt 3D orientations and (2) 2D rotations, while the blood oxygen level-dependent signal was recorded from visual cortices. Multivariate pattern analysis (MVPA) classification was utilized on functional magnetic resonance imaging (fMRI) data to find the relation between object orientation and ROIs in visual cortices.

key words Object orientation, 3D orientation representation, Grasping, Vision for action, functional magnetic resonance imaging, Multivariate pattern analysis

Contents

List of Figures

List of Tables

Chapter 1

Introduction

The function of object perception through 3D world is a fundamental of human vision. The ability to observe and manipulate object; such as looking and grasping a cup of coffee, requires such a sophisticate communication between multiple brain region relate to vision and action. One object manipulation of the brain that we are interested in is object orientation perception. Several studies investigated by using functional magnetic resonant imaging (fMRI) to decode the human brain for a better understanding of this function.

One hypothesis about the relation of vision and action was proposed and call "Two Stream hypothesis" by Melvin Goodale and David Milner [1]. This study introduced that the vision to action (dorsal stream) and vision for perception (ventral stream) are two different pathways of visual region but somewhat cooperate in our visual system. When we observed an object, some brain regions in a dorsal stream are activated for planning to take possible action such as visually guiding hand, adjusting hand to align with the object orientation, while the ventral stream perceives the object shapes, color, texture and other features that indicate its identity.

From grasping feature of an object, there are a number of studies that support the objects with the graspable feature are inclined to have activated the tools-network and some areas in IPS area [6, 7, 10, 18]. The representation can be as simple as an elongated shape which most manipulable tool-like object possessed.

In another aspect, the object orientation was studied widely in the 3D representa-

tion. Generally, the surface or slant shapes are used in several studies. In our previous studies [23, 24], the cortical representation of stereoscopic 3D surface was investigated and the result showed that some regions of interest (ROI) in intraparietal sulcus (IPS) had a tendency for 3D shape orientation classification. Since it is well known that IPS area, located in dorsal stream, is involved in vision for action.

In this study, we investigated the connection of 3D orientation and object that has action related feature by using stimuli representing real-world object in different orientations. We conducted an fMRI experiment and used the multivariate pattern analysis (MVPA) classification on the fMRI data. We were expected to produce a better 3D orientation classification to verify that the action related graspable feature has effected on objects orientation perception.

To be precise, The purposes of this study are clarified by the following:

1. Find the association between orientation and object relate to action
2. Investigate the generalized representation of 3D object orientation
3. Find the ROIs that relate to 3D object orientation classification

Chapter 2

Background Study

This chapter presents the background research related to this study. The content is divided into 3 parts; Two streams hypothesis, Grasping properties, and 3D orientation.

2.1 Two Streams Hypothesis

The discovery of two streams visual system (ventral and dorsal stream) in human brain has put a new aspect in neuroimaging studies. The ventral stream is involved in object identification perception and recognition which is known as visual for perception. Whereas, the dorsal stream is known for importance in visually guided action, object's spatial location relative to the viewer, in other words, visual for action. The dorsal stream was delicately studied by the past years study in the relation between visual and action [1].

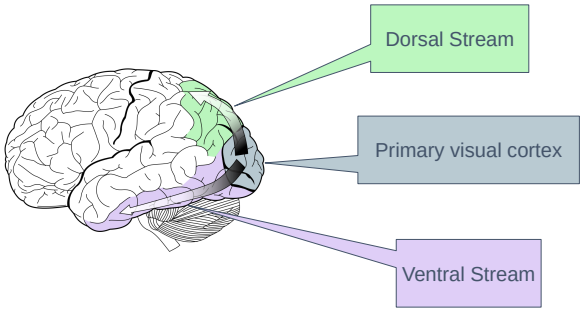

Fig. 2.1 The two streams illustration

One of the dorsal area functions discovered was the sensitivity to object orientation

changes in 2D rotation [4]. This study discovered that a region in the parieto-occipital cortex (dorsal stream) showed BOLD activity increasing to changes in object orientation, but insensitive for changing in object identity. In contrast to the dorsal stream, a region in temporo-occipital cortex (ventral stream) had high sensitivity activity in object's identity changes. The disassociation of orientation and identity is consistent with the general idea of dorsal stream function to object-directed action whereas the ventral stream has a critical role in object perception.

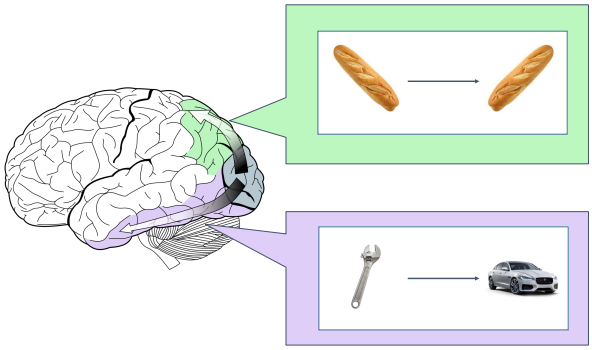

Fig. 2.2 Orientation and identity sensitivity of two streams

The object orientation sensitivity in dorsal stream was investigated further in a year later [6]. The idea proposed that if object orientation sensitivity in the dorsal stream does reflect such a potential for action, then this sensitivity should be specific to graspable objects. In their result showed the lateral occipito-parietal junction (lOPJ); a region within dorsal stream, tended to be sensitive to orientation changes for graspable stimuli; this region did not show orientation sensitivity for non-graspable stimuli. Therefore, it appears that the sensitivity to orientation changes in this region is specific to graspable objects, presumably because such changes affect the affordances of graspable but not non-graspable objects.

The role of right parietal lobe in object identification and the ability to interpret object orientation was investigated by Harris and colleagues[9]. They used transcra-

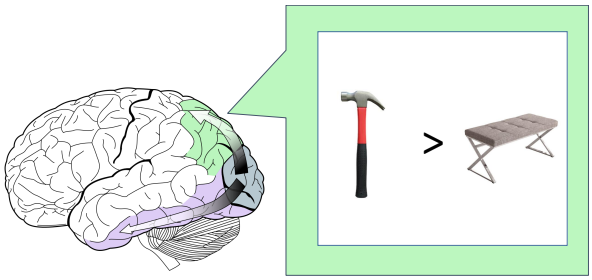

Fig. 2.3 The dorsal stream has more specific sensitivity on graspable objects than non graspable objects

nial magnetic stimulation (TMS) to briefly interfere with ongoing cortical activity while subjects were executing either object identification tasks or object orientation judgment tasks. The result showed that the right parietal lobe region impaired orientation judgments by TMS, but promoted object identification, compared to TMS applied to a brain vertex control site. This pattern of results support the importance of the parietal lobe (dorsal stream) in processing the spatial attributes of objects, but not their identity.

In a recent study, the dorsal stream object-based representations were questioned whether they were dissociable from ventral stream representations and whether they play a functional role in object recognition [11]. The patients with ventral stream impairments in object recognition participated in the fMRI experiments. The patients still revealed residual sensitivity to object-based structural information despite their significant impairments in object perception. These findings suggest that there is sufficient crosstalk between dorsal and ventral cortices. The object coarse structural information representations in dorsal cortex can be computed independently from those in ventral cortex.

2.2 Grasping and Tools

From dorsal stream, we could refer that the major attributes in vision for action that relate to object orientation are the action to be performed on object (i.e. grasping) and the affordance related features (e.g. handle) for grasping.

The grasping property in dorsal stream was studied in motor system approached [7]. This study demonstrated that activity within the human anterior intraparietal sulcus (hAIPS) is modulated according to different types of grasp with more active for precise grasping than for whole hand independently of stimulus size. Thus, This is evidence in humans that the dorsal premotor cortex is involved in grasp planning and execution offers a considerable benefaction to the discussion on the topic of visuomotor grasp in humans.

In the same year, Valyear and colleagues studied the tool-related fMRI activity within the intraparietal sulcus [8]. Their study aimed to evaluate whether this tool-related intraparietal activity could be accounted for by the graspable nature of tools or whether it was due to additional factors such as the functionality of tools. The activation of naming task within a discrete region of the left anterior intraparietal cortex was found higher for tools than for graspable objects but did not differ between graspable and non-graspable objects. These findings indicate that the anterior end of the left IPS is likely to be tool-selective area and is both separable from the grasp-related intraparietal activity and, The process of grasping affordances is not reflected by it. Alternatively, this activity may relate to learned motor representations associated with the familiarity of tools.

In a different approach, the psychological experiments about the existence of a pure physical affordance of object orientation were studied [5]. The behavioral effects found from the experiment were larger and more robust when the object tends to be graspable,

and the orientation was in-depth particular that is oriented to be slant outward toward a certain hand of viewer.

Years later, the study from Sakuraba and colleagues[10] proposed that human dorsal stream processes the category for tools and examine what attributes of tools are processed in the dorsal stream. The result suggested that the elongated shape of a tool-like object indicates as the prime attribute which process in dorsal area.

Fig. 2.4 The elongated shape indicates prime attribute for process tool-like objects in dorsal stream

The elongated shape of tools was studied later by Macdonald and colleagues [18]. The low-level feature of both tools and non-tools tends to differ. In their experiment, To maximize the potential for action, participants saw real-tools and non-tools as opposed to pictures of them. The results showed that, even after the low-level differences between tools and non-tools were controlled, tools evoked more activation in the tool network, located on left-lateralize network of the brain, as well as in sensorimotor areas. The orientation of the tool handles did not interfere effects within these sensorimotor areas and when passively viewed tools, even without an intent to act, functional networks are automatically stimulated.

In another aspect, the various properties of objects(shape, size, and elongation) influence the way human grasp them. In the study from Fabbri and colleagues[20], the fMRI was performed to find the representation of object properties and hand configura-

tion in the human brain. The result showed the object elongation was the most strongly represented object feature during grasping and was coded preferentially in the primary visual cortex as well as the anterior and posterior superior parieto-occipital cortex. This neural evidence reinforced the previous study[10] about elongation represented grasping properties of object even in passively view task.

The action of grasping can be sort into whole hand and precision grasp then applied in experiments of study by Di Bono and colleagues [13]. Their experiment used MVPA on fMRI data to evaluate whether regions of the frontoparietal network discriminate between reaching-only and reach-to-grasp actions, natural and constrained grasping, different grasp types, and object sizes. The task participants required to perform were either reaching-only movements or two reach-to-grasp types (precision or whole hand grasp) upon spherical objects of different sizes. Their results showed that, independently from object size, the grasp type (whole hand or precision grasp) could be discriminated by the linear classifier in a wide frontoparietal network of both hemispheres.

2.3 3D Orientation

The previous sections suggest the relevancy of action and object orientation in dorsal stream and other related areas. However, the 3D perception of the object has been studied in parallel for our background work as well.

The representation of 3D orientation was previously studied in the 3D slanted surface to emphasis on 3D perception only. The binocular disparity was one of the stimulus cues that is well known for 3D vision research. Together with texture cues, the study of Murphy and colleagues [14] found that even the two cues are qualitatively very different. There exist a piece of evidence suggests that representations of surface tilt from each of these cues coincide at the single-neuron level in higher cortical areas. The discriminabil-

ity of fMRI responses to two slant angles was analyzed by using MVPA classification with both visual cues. The result did suggest that the area V3B/KO is intricately involved in the integration of qualitatively dissimilar depth cues. In same year's study from Dövencioğlu and colleagues [15], the fMRI responses from area V3B/KO were found more discriminable when disparity and shading concurrently signaled depth, in line with the predictions of cue integration. Their result was later revealed a generalized 3D depth representation in dorsal visual cortex from different cues combined.

The full 3D orientation visual encoding was the focus on a study by Rosenberg and colleagues [16] and the caudal intraparietal area (CIP) are suggested to be involved. With 3D representation of the slant and tile surface, the area CIP is equally represented them. Additionally, some neurons in CIP are found to represent the third rotational degree of freedom that determines the orientation of the image pattern on the planar surface. To sum up, the results suggest that CIP has a critical role in the encoding of all three rotational degrees of freedom specifying an object's 3D spatial orientation.

In our previous studies [23, 24], The cortical representation of stereoscopic 3D surface was in early visual areas and higher areas. The random-dot stereogram of hemicylindrical convex and concave surfaces was used as the stimuli. Among the results, the classification of horizontal versus vertical orientation on same type convex and concave shape had shown high classification accuracy in some ROIs in IPS areas, which are from the dorsal stream. This showed that IPS areas had a tendency for 3D orientation classification.

The recent study used a different viewpoint to identified target status changes [25]. The stimuli of 3D abstract objects were made and presented in different orientation and identity as a part of the experiment. In the viewpoint task, the result showed a high target detection rate in IPS areas which consistent with the past work in this ROI.

In our study, the fMRI experiment was conducted to find the association between

2.3 3D Orientation

3D object orientation and ROIs in visual area by applied the new stimuli represent 3D objects that relate to action task (e.g. grasping, holding) instead of a 3D surface from the previous study which expect to provide the evidence of relation between 3D orientation and object relate to action.

Chapter 3

Multivariate Pattern Analysis Theory

The prominent brain decoding methods, MVPA, was described in this chapter by illustrating the application of machine learning principle on the fMRI functional data and permutation test.

3.1 Introduction of Multivariate Pattern Analysis (MVPA)

In traditional ways of analysis in fMRI study, the BOLD signal is measured to detect changes in brain activity of each condition given it. For example, when people heard a sound, the areas in auditory system of the brain are active and BOLD signal will have high contrast from the previous non-hearing base state. The method to analyze BOLD signal require using general linear model (GLM) on each voxel within the auditory region. The GLM can only analyze single voxel at the time and cannot detect any activity pattern of several voxel together[17].

James Van Loan Haxby and colleagues propose the multivariate pattern analysis (MVPA) or multi-voxel pattern analysis method in 2001 [2, 12]. Their study introduced the methods to handle the multiple voxels from fMRI data as a pattern and decode information according to their experiment's conditions. In a few years later, Kenneth

A. Norman and colleagues had re-introduced the pattern-classification algorithm for MVPA [3]. Their article described the features of MVPA methods to characterize neural coding and information processing in domains ranging from visual perception to memory search.

MVPA is fundamentally considered the multi-voxel pattern as a pattern in high-dimensional space and uses pattern classification to decode the information reside in themselves. The procedures of MVPA usually compose of 4 steps; feature selection, pattern assembly, classifier training, and cross-validation.

3.1.1 Feature Selection

In this first step, the voxels included in the analysis are decided. The whole-brain voxels are applicable but the dimension of data can be overwhelming. One of the common methods is to select a region of interest voxels base(ROI-base) for more specific analysis. Another approach is calculating the univariate/voxel-wise statistics. Our study applied the ROI-base analysis and used the raw data trial extracted from the onset with 3 repetition time (TR) or 6 s delay according to the hemodynamic peak/plateau behavior of spreading out across several time points after the condition onsets time[Figure 3.1]. The baseline from fixation signal was subtracted from raw data trial at 2 TRs before the trial onset to obtain more robust trial data.

3.1.2 Pattern Assembly

The features are labeled for each condition of the experiment in this step. The labeled pattern assembles data composes of vectors of multiple eigenvalues. In each experiment condition, there are multiple labeled data for training and one labeled data can cover a long period of TR. In our experiment, we covered 3 TRs[Figure 3.1, 3.2].

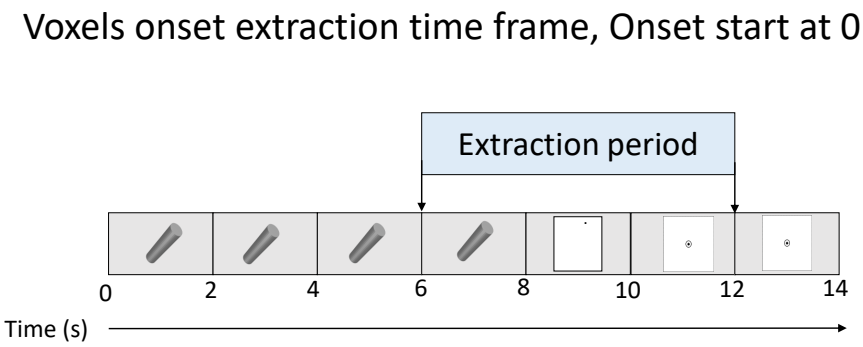

Fig. 3.1 The extraction time for our study: With TR = 2 s, The trial was extract 3 TRs (6 s)later from the start of onset time due to hemodynamic peak delay

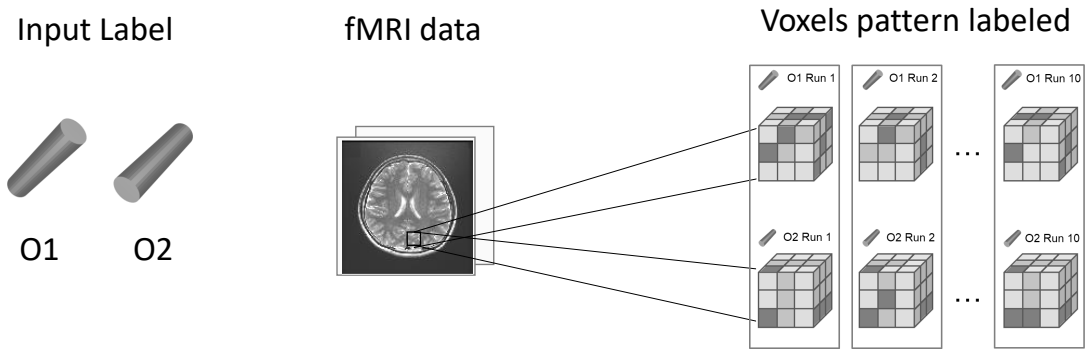

Fig. 3.2 The extracted patterns labeled according to experiment's condition

3.1.3 Classifier training

The classifier is created from the division of labeled data set into training data and testing data. The classifier trains from training data and is evaluated by using testing data. Classifiers which generally use in MVPA are nearest neighbor, support vector machine (SVM), and neural network. Our study used SVM classifier.

3.1.4 Cross-validation

The total number of data set is limited causing the cross-validation to be performed for a good estimation of the result. In our study, we chose Leave-one-run-out cross-validation (LORO-CV) method. In leave-one-run-out cross-validation, the classifier is trained using the training set and then tested using the test set to verify performance. This procedure is repeated for each run to get at the end an averaged performance of the total run[Figure 3.3].

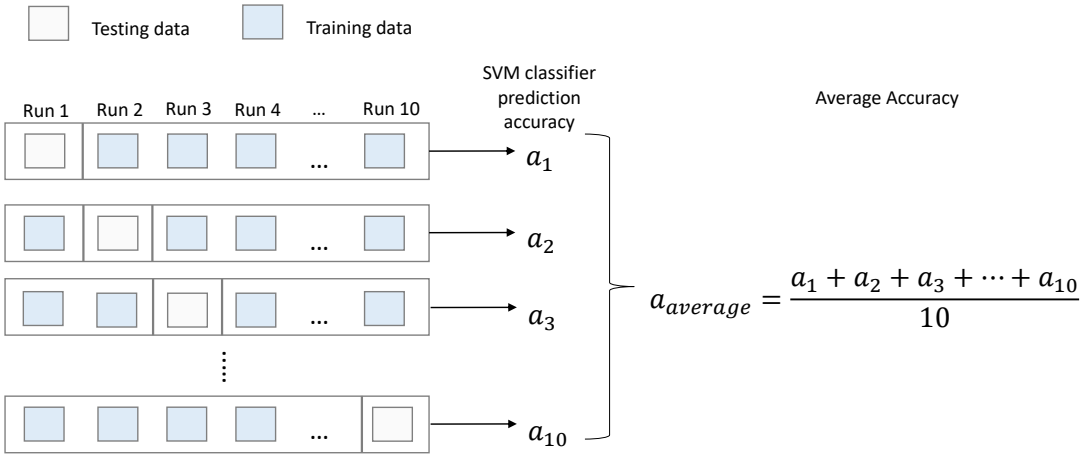

Fig. 3.3 cross-validation methods of the experiment

3.2 Permutation test

The basic principles of the permutation test are similar to the MVPA (non-permuted) classification [21, 22]. The main difference is that: in the permutation test, all labels were permuted before cross-validation performed each time and repeated permutation and classification for 1000 times in our study case. The detailed procedures are as follows:

1. For each data set of one participant:

1)Permute the labels in the data set.

2)Perform leave n data out cross-classification.

3)Repeat step 1) and 2) for 1000 times and get an accuracy vector $\vec{\alpha}_{(i,j)}$ (i indicates the i^{th} participant and j indicates data set D_j $(1 \leq i \leq 5, 1 \leq j \leq 6)$, each element $\alpha_{(s,t)}$ in $\vec{\alpha}_{(i,j)}$ indicates classification accuracy of t^{th} permutation test on data set $s(1 \leq t \leq 1000, 1 \leq s \leq 6)$[Figure 3.4 (a) (b)]).

2. For each participant i, we calculated the average value of accuracy on 4 data sets and get vector $\vec{\beta}_i(1 \leq i \leq 5)$ [Figure 3.4 (c)]
3. Average the $\vec{\beta}_i(1 \leq i \leq 5)$ across all participant and we get vector $\vec{\gamma}$ [Figure 3.4 (d)]. Thus, a distribution of classification accuracy was created and the upper 99.6% centile was used as the chance level of classification based on the distribution.

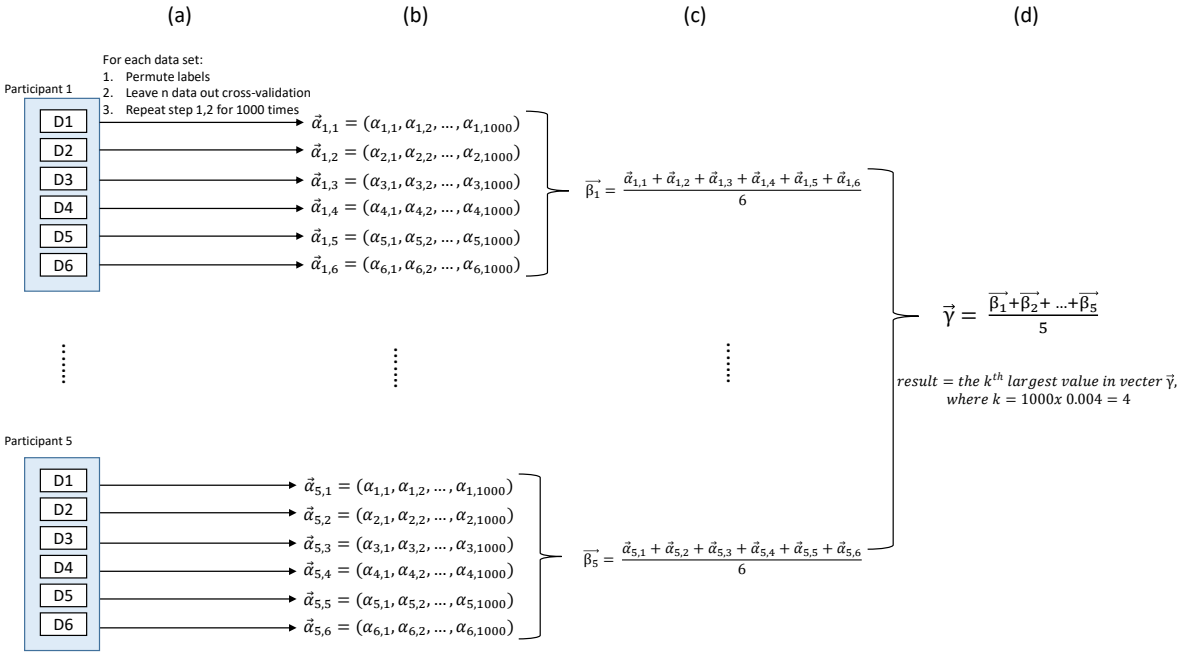

Fig. 3.4 The procedure of permutation test

Chapter 4

Experiment Design and Analysis Methods

This chapter represents the details of the methods used in our study. The content includes recruited participant details, stimuli setup, experiment design, fMRI data acquisition, and analysis procedure.

4.1 Participant

Five participants (2 females) between the ages of 20 and 24 were recruited from Kochi University of Technology, had normal or correct-to-normal vision. The background reports had none of any mental illness or neurological disease background. The participants were paid for their involvement and this study was carried out according to Human Research Ethics Committee of Kochi University of Technology with solid informed consent documents from all participants.

4.2 Stimuli

Pre-rendered 3D object images were presented on a screen by the JVC D-ILA video projector. The images were projected on a translucent screen in between an fMRI magnet coil. The participants observed stimuli through a pair of slant mirrors above the head coil. The screen resolution was set to 1920 x 1080 pixels.

The pre-rendered 3D objects were presented in 2D gray-scale images. The 3D orientation perception was defined by using a perspective of pictorial depth cue. All stimuli were made by free license 3D software, Blender. There were three types of stimuli categorized by the type of action to be performed onto object. The three types of stimuli (i.e abstract cylinder shape, coarse grip axe, and precision grip ballpoint pen) were presented at four orientation around horizontal and vertical axis (x-axis, y-axis) as following pairs; O1(45°, 45°), O2 (45°, -45°), O3 (-45°, 45°), O4 (-45°, -45°)[Figure 4.1].

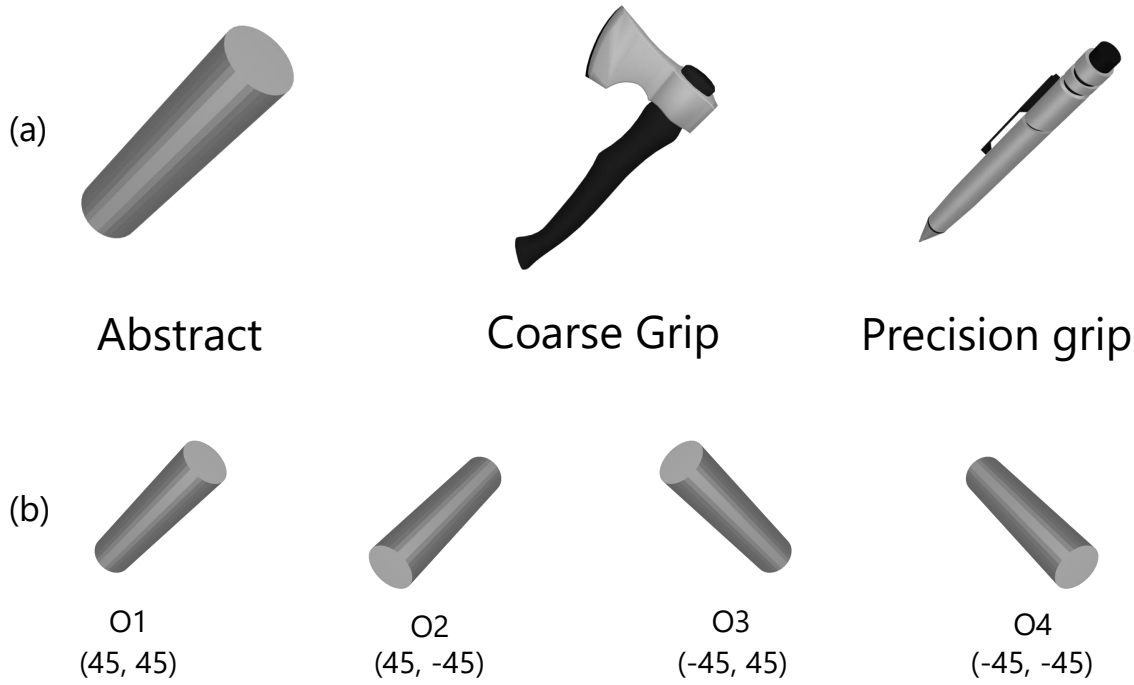

Fig. 4.1 (a) Stimuli and (b) Orientations illustration

4.3 Experiment design

The stimuli were presented to participants in random order from 12 conditions (3 types x 4 orientations) by using block design. Each stimuli trial was repeated for 20 times and the total stimuli trials are 240 trials (3 types x 4 orientations x 20 repetitions).

In each stimuli trial, The stimuli were shown for 8000 ms and were flickering during

this period for 500 ms repetitively [Figure 4.2]. After each stimulus block, a single square dot appeared on the position of object's end ('near' or 'far' depth perceived) as a judgment task for 2000 ms [Figure 4.3]. The participants were required to press the corresponding assigned button of each depth position of the object's end. The response task was followed by a 4000 ms fixation block.

The 6000 ms fixation block was shown at the beginning and the end of each run, the total time of each run was 348 s. Each session had 10 runs.

During the response task, the answers were recorded in each run to calculate the perception performance of each subject. The tasks without any answer are discarded from the calculation.

All participants were required to keep their head still and look at the fixation in the center of the screen. Any runs extravagant head movement were discarded. The extravagant head movement was interpreted as the head movement of more than 2 mm or head rotation more than 2 ° from the first slice in each run.

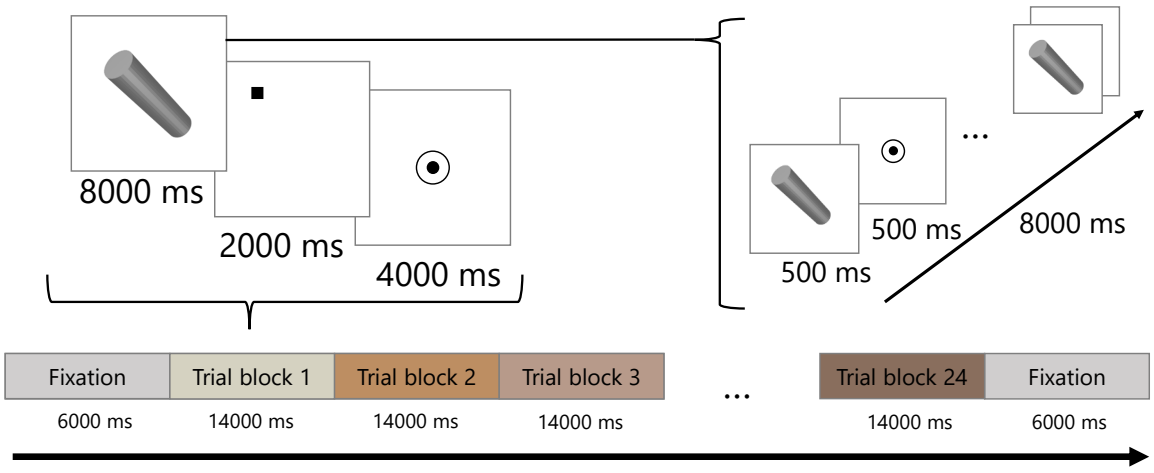

Fig. 4.2 The experiment block design overview

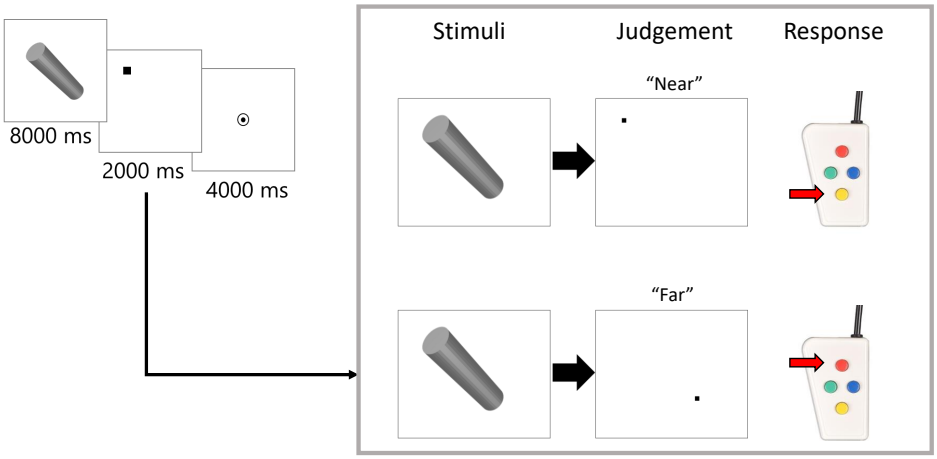

Fig. 4.3 The judgment task overview

4.4 fMRI data acquisition

All scanned image was performed using 3 Tesla Siemens MAGNETOM Skyra MRI scanner at the Brain Communication Research Center of the Kochi University of Technology. MRI compatible foam pads were used to fixed participants head to reduce excessive movement. A high resolution T1-weighted anatomical scan (1 mm^3) was acquired for the participants and regions of interest(ROI) were localized in the previous study's sessions [23, 24]. In each run of experiments, BOLD signals were measured with an echo-planar imaging (EPI) sequence sequence (echo time [TE]: 58 ms; repetition time [TR]: 2000 ms; number of volumes per run: 174; slice thickness: 3 mm; slice acquisition order: interleaved) from 34 slices covering the visual cortex, posterior parietal cortex, and posterior temporal cortex. For the structural data, T2-weighted structural image of each participant was retrieved in a 2.5 minutes run and was recorded before the first corresponding EPI data in one session. T2-weight structural data were used as reference slices of the EPI data motion correction and co-registration between T1-weighted anatomical images and EPI data in native anatomical space. After that, all data were converted to Talairach coordinates for the trial extraction of MVPA.

4.5 Region of interest (ROI)

All regions of interest of were initially made individually from all localizers adopted in previous studies [23, 24, 19] in which we have used the same participants as the previous research. Both left and right hemispheres pattern were used for creating the classification sample data.

ROIs covered 12 regions as shown in the following[Figure 4.4]:

1. Early visual area: V1, V2, V3d, V3v, V3A
2. Higher ventral area: lateral occipital complex (LOC)
3. Higher dorsal area: human motion complex(V5/hMT+), kinetic occipital area(V3B/KO), V7
4. Intraparietal sulcus (IPS) areas: ventral intraparietal sulcus (VIPS), parieto-occipital intraparietal sulcus (POIPS), dorsal intraparietal sulcus (DIPS)

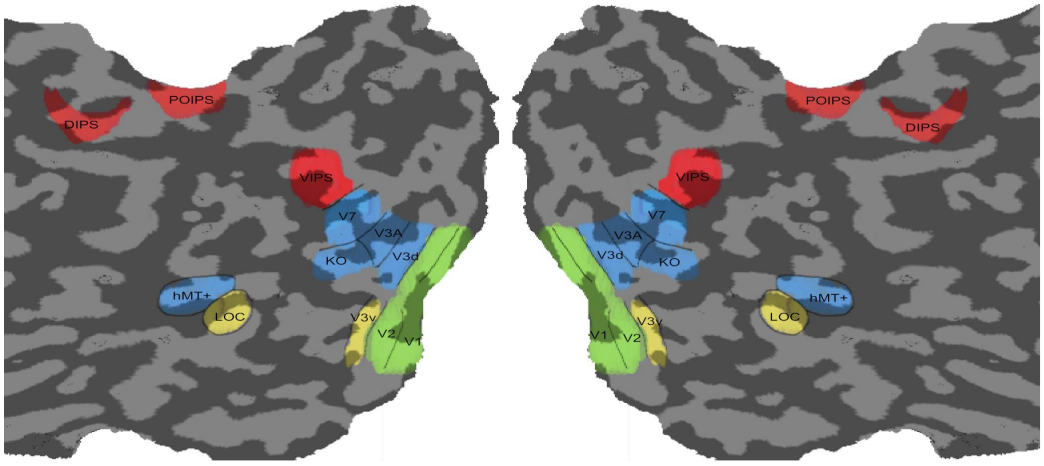

Fig. 4.4 Region of interest's cortical flattening

4.6 Data Analysis

After the EPI data were collected, preprocessed and co-registered with T1-weighted scan through BrainVoyager software, we performed MVPA for the EPI data for each ROI with MATLAB. A linear support vector machine (SVM) was used as a classifier for MVPA. The classifier pairs were arranged into 2 types, (1) 3D orientation classification composed of (O1, O2) and (O3, O4) pairs, (2) 2D orientation classification composed of pairs of (O1, O4), (O2, O3), (O1, O3), and (O2, O4).

All classifications were divided into 3 categories according to the method of handling the sample data as the following:

1. Same-type stimuli classification: training and testing within the same stimulus type
   (a) Abstract only classification
   (b) Coarse only classification
   (c) Precision only classification
2. Transfer-type stimuli classification: training in one stimulus type and testing with another stimulus type, and vice versa
   (a) Abstract-coarse classification
   (b) Coarse-precision classification
   (c) Precision-abstract classification
3. Generalized stimuli classification: training the combined stimulus type as one sample data and testing within the same stimulus type

In each classification, the leave-one-run-out method was used to assess the performance of MVPA classification. The data for test were separated by one run while the rest of data from other runs were used as training data. This method was repeated for total of number of all runs, then averaged each iteration accuracy to find the accuracy of a single participant. The classification accuracies of all across participants were

averaged for each ROI.

The statistical significance of MVPA was performed with permutation test [21]. Each pattern was permutated then was used as a training data on real testing data, the accuracy across participants was averaged as a permutation accuracy and this permutation test was repeated 1000 times on each ROI. The baseline for statistical significance was 99.6 percentile (one-tailed, 12 ROIs).

The calculated scores from response task's answers are evaluated as the perception performance test by each stimulus. The one-way analysis of variance (ANOVA) was used to find the difference of 3D orientation perception between three stimulus types.

Chapter 5

Result

This chapter presents the result from 3D objects orientation classification. First, the analysis result of perception performance is presented. Next, the MVPA results are shown by 3 categories according to the method of handling the sample data; same-type stimuli classification, transfer-type stimuli classification, and generalized stimuli classification.

5.1 Perception performance test

The significant test was done by using ANOVA. the result of perception performance test are shown in [Table 5.1]. We performed a single factor ANOVA on the same orientation across 3 stimuli types (abstract, coarse grip, and precision grip). Each orientation, the results showed no significant difference among the different stimuli types (O1 to O4). The ANOVA results are as following; O1 group(A1,C1,P1) $F(2,12) = 0.18$, O2 group(A2,C2,P2) $F(2,12) = 1.27$, O3 group(A3,C3,P3) $F(2,12) = 0.33$, O4 group(A4,C4,P4) $F(2,12) = 0.13$, while the average accuracies of each stimulus are shown in [Figure 5.1]. All ANOVA results did not reject the null hypothesis at $\alpha = 0.05$, $F(2,12) = 3.8853$.

5.1 Perception performance test

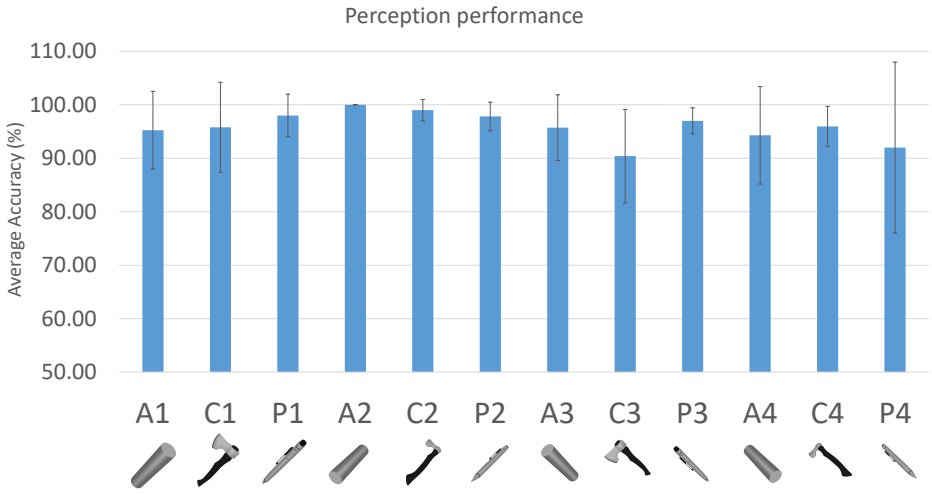

Fig. 5.1 Perception accuracy (%) average from all participants.

Table 5.1 Perception performance from all participants

	Perception accuracy (%)					
Participant	P1	P2	P3	P4	P5	average
A1	81.25	100.00	100.00	100.00	95.00	95.25
C1	100.00	78.95	100.00	100.00	100.00	95.79
P1	100.00	90.00	100.00	100.00	100.00	98.00
A2	100.00	100.00	100.00	100.00	100.00	100.00
C2	100.00	100.00	100.00	100.00	95.00	99.00
P2	94.12	95.00	100.00	100.00	100.00	97.82
A3	84.21	94.44	100.00	100.00	100.00	95.73
C3	77.78	84.21	100.00	100.00	90.00	90.40
P3	100.00	95.00	95.00	100.00	95.00	97.00
A4	76.47	100.00	100.00	100.00	95.00	94.29
C4	94.74	95.00	100.00	100.00	90.00	95.95
P4	60.00	100.00	100.00	100.00	100.00	92.00

5.2 Same-type Classification

The same-type classification implemented training and testing data within the same stimuli type. This classification category composed of 3 sub-categories as follows: abstract only classification, coarse only classification, and precision only classification.

5.2.1 Abstract only classification

The abstract only classification predictions accuracies from all pairs were presented in [Table 5.2] and illustrated in [Figure 5.2] and [Figure 5.3] in bar charts. The error bars in both figures represented the standard error of the mean from each classification. The red dotted horizontal lines marked the chance level baseline generated from permutation test. The lines level indicated upper 99.6% centile of the distribution of permuted data from the test. The black dotted horizontal line specified 50% accuracy level.

In 3D orientation [Figure 5.2], the first classification pair's (O1, O2) prediction accuracies from all ROI showed no significance or high accuracy. But in (O3, O4), the result showed significantly high accuracy in KO and VIPS area with 65.25% and 63.88% [Figure 5.2]. In some other areas had high accuracy but failed to pass the chance level baseline by each lower standard error of the mean.

In 2D orientation [Figure 5.3], the overall result showed high accuracy in V2 and V3v especially in the result from (O2, O4) which had high accuracy and passed the baseline in V3v with 65.63%. In other areas such as V1, V2 V3A, KO, hMT+, and VIPS, the results showed high prediction accuracy in (O2, O4) but failed to pass the baseline. The rest of classification pairs ((O2, O3), (O1, O3), (O1, O4)) showed no significance.

Table 5.2 Prediction Accuracy (%) Results from Abstract Only

ROI	Prediction accuracy (%)					
	3D Orientation		2D Orientation			
	(O1, O2)	(O3, O4)	(O2, O3)	(O1, O3)	(O1, O4)	(O2, O4)
V1	61.50	57.25	53.25	60.50	56.13	62.00
V2	54.38	65.50	58.63	63.13	52.25	63.25
V3d	51.88	57.00	49.50	51.88	46.00	53.50
V3v	56.88	62.63	53.88	61.25	49.63	**65.63**
V3A	50.13	60.00	52.50	51.88	51.63	61.13
V7	55.13	62.25	48.25	61.25	60.50	51.75
KO	62.50	**65.25**	55.75	59.00	54.50	61.50
hMT+	49.38	56.50	54.00	54.25	52.13	59.75
LOC	40.13	52.25	49.88	47.25	49.88	50.00
VIPS	48.50	**63.88**	58.25	56.13	52.88	59.75
POIPS	48.50	56.25	49.13	50.50	58.50	55.25
DIPS	49.63	52.00	42.25	50.63	50.25	51.13

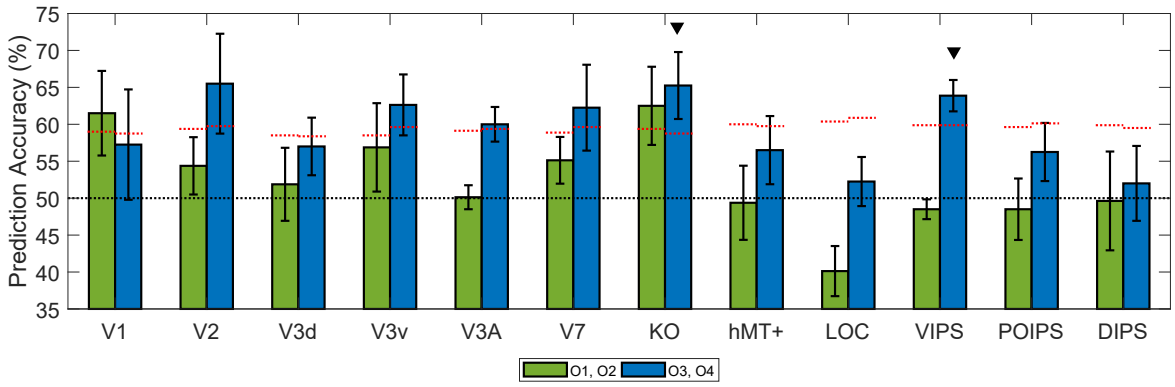

Fig. 5.2 Abstract only 3D orientation classification accuracy each ROI

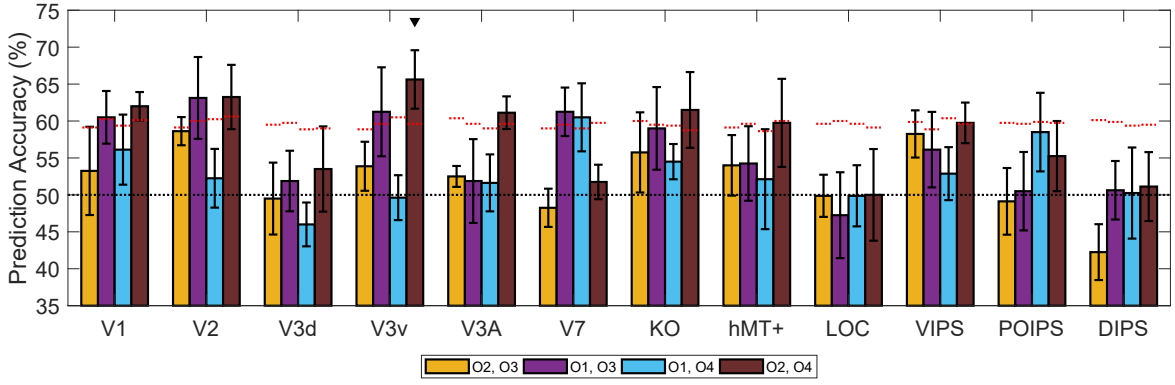

Fig. 5.3 Abstract only 2D orientation classification accuracy each ROI

5.2.2 Coarse only classification

The coarse only classification predictions from all pairs were presented in [Table 5.3] and illustrated in [Figure 5.4] and [Figure 5.5] in bar charts. The error bars in both figures represented the standard error of the mean from each classification. The red dotted horizontal lines marked the chance level baseline generated from permutation test. The lines level indicated upper 99.6% centile of the distribution of permuted data from the test. The black dotted horizontal line specified 50% accuracy level.

In 3D orientation [Figure 5.4], the results from V1, V2, V3v and KO presented a high accuracy on both classification pairs ((O1, O2), (O3, O4)) but, only the classification of area V1 that passed the baseline by lower standard error of the mean in (O1, O2) with accuracy of 62.5%. In contrast, the LOC and VIPS areas had relatively low accuracy on both classification pairs.

In 2D orientation [Figure 5.5], the results from V1, V2, V7, and KO showed high accuracy in some classification pair but only the result of V1 passed the baseline in (O2, O3) with an accuracy of 65.38%. The other ROIs had low accuracy and failed to pass the baseline.

Table 5.3 Prediction Accuracy (%) Results from Coarse Only

ROI	Prediction accuracy (%)					
	3D Orientation		2D Orientation			
	(O1, O2)	(O3, O4)	(O2, O3)	(O1, O3)	(O1, O4)	(O2, O4)
V1	**62.50**	59.00	**65.38**	56.50	60.75	61.63
V2	58.13	61.75	52.88	65.00	59.94	**63.00**
V3d	57.88	53.88	51.75	61.00	55.88	57.75
V3v	58.00	59.13	53.63	57.00	58.56	59.13
V3A	53.63	55.50	49.88	52.25	54.56	55.38
V7	56.75	55.75	53.00	61.13	56.25	50.88
KO	58.38	60.50	57.75	54.00	59.44	63.50
hMT+	56.25	53.50	51.63	48.38	54.88	49.00
LOC	50.88	46.50	49.63	47.25	48.69	52.50
VIPS	53.00	48.88	56.25	55.50	50.94	54.50
POIPS	46.25	53.13	46.88	52.25	49.69	53.75
DIPS	47.50	49.50	40.50	45.63	48.50	44.63

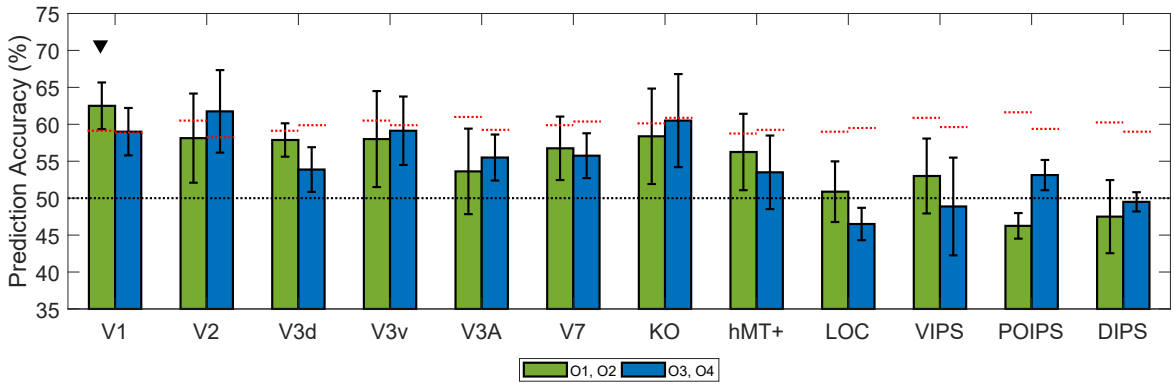

Fig. 5.4 Coarse only 3D orientation classification accuracy each ROI

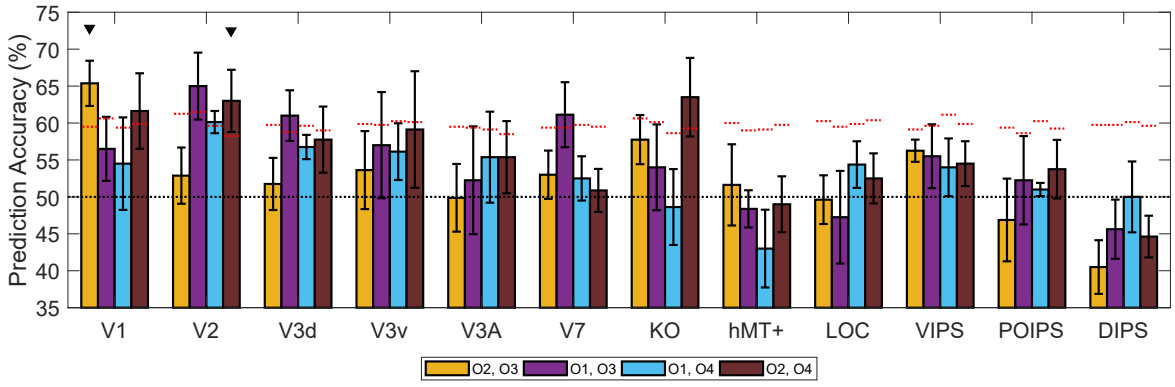

Fig. 5.5 Coarse only 2D orientation classification accuracy each ROI

5.2.3 Precision only classification

The precision only classification predictions from all pairs were presented in [Table 5.4] and illustrated in [Figure 5.4] and [Figure 5.5] in bar charts. The error bars in both figures represented the standard error of the mean from each classification. The red dotted horizontal lines marked the chance level baseline generated from permutation test. The lines level indicated upper 99.6% centile of the distribution of permuted data from the test. The black dotted horizontal line specified 50% accuracy level.

In 3D orientation [Figure 5.6], the pair (O1, O2) result from V3d area showed high accuracy and pass the baseline by the lower standard error of the mean with the accuracy of 65.63% while other areas show low accuracy and no significance. In the pair (O3, O4), most of the ROIs showed significantly high accuracy and pass the baseline by the lower standard error of the mean. The considerably significant ROIs included V2, V3A, V7, KO, hMT+, LOC, VIPS, POIPS, and DIPS with accuracies at 62.75%, 64.63%, 68.00% , 70.63%, 64.13%, 61.00%, 70.13%, 66.75%, and 66.88% respectively.

In 2D orientation [Figure 5.7], the results from (O2, O3) and (O1, O3) showed a low accuracy across all ROIs. None of the ROI's has significant prediction accuracy. On the contrary, the result from (O1, O4) and (O2, O4) showed distinctively high prediction accuracy above the chance level baseline by the lower standard error of the mean in most ROIs. In (O1, O4), the high accuracy results were from V2, V3d, V3v, V3A, V7, KO, hMT+, LOC, VIPS, POIPS, and DIPS with accuracies at 62.13%, 65.00%, 63.13%, 63.38%, 64.50%, 67.00%, 58.38%, 64.75%, 58.63%, 61.25%, and 59.88%.

Table 5.4 Prediction Accuracy (%) Results from Precision Only

ROI	Prediction accuracy (%)					
	3D Orientation		2D Orientation			
	(O1, O2)	(O3, O4)	(O2, O3)	(O1, O3)	(O1, O4)	(O2, O4)
V1	50.75	57.75	57.00	46.00	57.63	56.50
V2	55.75	**62.75**	54.13	53.38	**62.13**	**62.50**
V3d	**65.63**	61.25	47.88	47.38	**65.00**	**66.13**
V3v	58.75	58.63	50.50	56.63	**63.13**	**61.88**
V3A	57.25	**64.63**	43.75	45.00	**63.38**	**64.25**
V7	48.75	**68.00**	53.88	48.00	**64.50**	**66.25**
KO	59.38	**70.63**	54.38	53.38	**67.00**	**71.00**
hMT+	46.38	**64.13**	48.13	49.38	**58.38**	**64.75**
LOC	48.50	**61.00**	45.13	45.25	**64.75**	**63.63**
VIPS	49.13	**70.13**	44.63	52.50	**58.63**	**64.00**
POIPS	48.00	**66.75**	53.38	46.88	**61.25**	**64.63**
DIPS	44.63	**66.88**	55.25	49.75	**59.88**	**63.63**

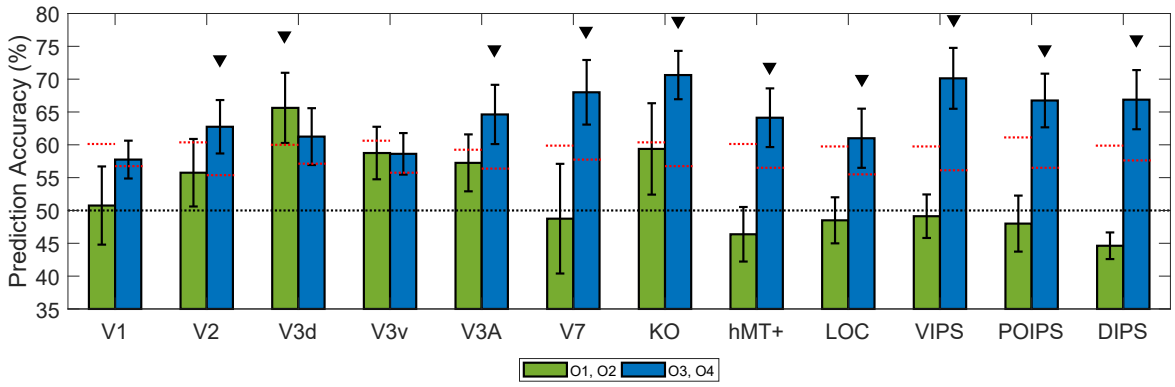

Fig. 5.6 Precision only 3D orientation classification accuracy each ROI

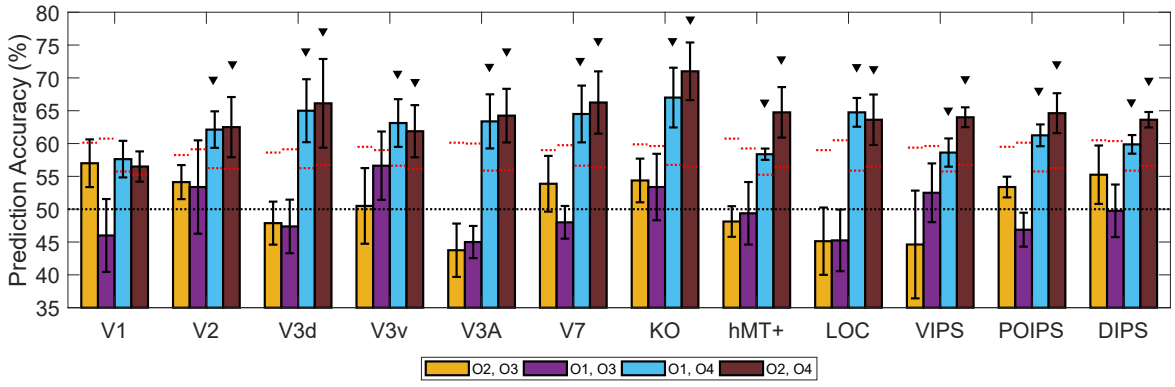

Fig. 5.7 Precision only 2D orientation classification accuracy each ROI

5.3 Transfer-type Classification

The transfer-type classification implemented training data and testing data with different stimuli types. This classification category composed of 3 sub-categories as follows: abstract-coarse classification, coarse-precision classification, and precision-abstract classification.

5.3.1 Abstract-coarse classification

The abstract-coarse classification predictions from all pairs were presented in [Table 5.5] and illustrated in [Figure 5.8] and [Figure 5.9] in bar charts. The error bars in both figures represented the standard error of the mean from each classification. The red dotted horizontal lines marked the chance level baseline generated from permutation test. The lines level indicated upper 99.6% centile of the distribution of permuted data from the test. The black dotted horizontal line specified 50% accuracy level.

In 3D orientation [Figure 5.8], the pair (O1, O2) result from V2 area showed high accuracy and passed the baseline by the lower standard error of the mean with 61.13% prediction accuracy. The area KO showed moderately high accuracy with 59.88% but failed to exceed the baseline, while other areas showed low accuracy and no significance. In the pair (O3, O4), all ROIs showed accuracy below baselines by the lower standard error of the mean. Both classification pairs accuracies from IPS areas and dorsal areas were around the chance level (50%).

In 2D orientation [Figure 5.9], the overall result showed accuracies at around chance level (50%). The prediction accuracies from V1, V2, KO, and POIPS were above the baseline in some classification pairs but failed by the lower standard error of the mean.

Table 5.5 Prediction Accuracy (%) Results from Abstract-coarse

ROI	Prediction accuracy (%)					
	3D Orientation		2D Orientation			
	(O1, O2)	(O3, O4)	(O2, O3)	(O1, O3)	(O1, O4)	(O2, O4)
V1	51.56	57.00	52.13	56.63	51.63	58.56
V2	**61.13**	57.38	50.00	53.81	53.69	59.50
V3d	52.06	53.25	51.06	53.63	50.13	52.25
V3v	55.00	54.25	51.63	56.69	54.06	54.94
V3A	50.13	54.13	48.75	53.25	53.06	48.81
V7	50.94	47.31	49.19	54.19	52.69	45.69
KO	59.88	57.19	45.13	52.50	50.00	59.44
hMT+	49.88	51.81	50.13	46.88	52.50	51.38
LOC	48.44	47.00	50.75	47.75	50.88	52.44
VIPS	50.31	51.50	46.31	52.13	47.38	48.38
POIPS	48.25	51.75	52.63	60.38	49.00	46.56
DIPS	47.69	54.00	50.00	49.69	50.81	52.94

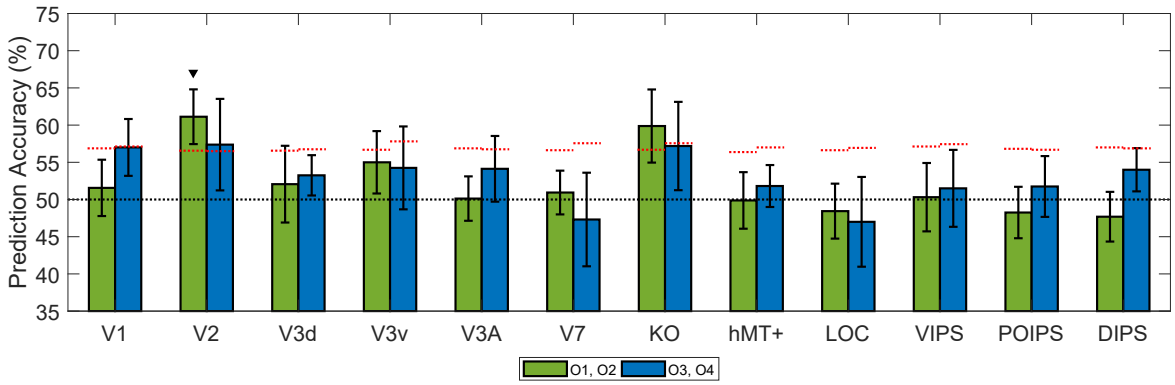

Fig. 5.8 Abstract-coarse 3D orientation classification accuracy each ROI

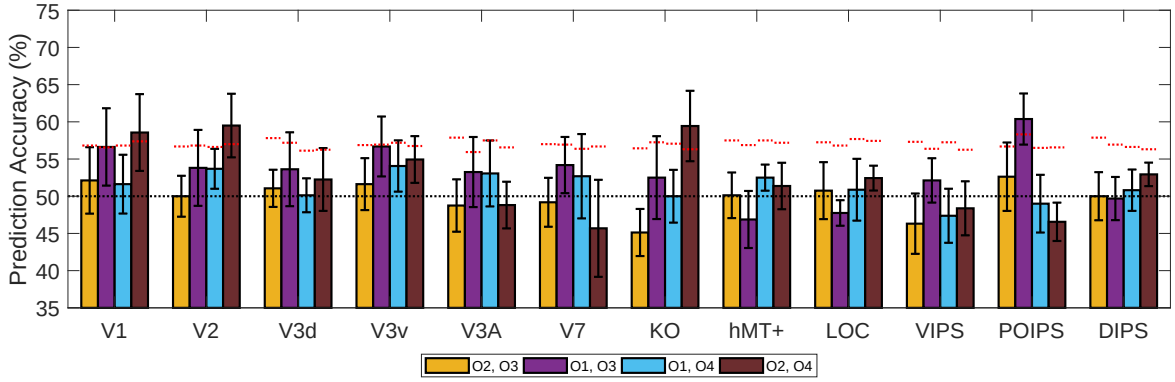

Fig. 5.9 Abstract-coarse 2D orientation classification accuracy each ROI

5.3.2 Coarse-precision classification

The coarse-precision classification predictions from all pairs were presented in [Table 5.6] and illustrated in [Figure 5.10] and [Figure 5.11] in bar charts. The error bars in both figures represented the standard error of the mean from each classification. The red dotted horizontal lines marked the chance level baseline generated from permutation test. The lines level indicated upper 99.6% centile of the distribution of permuted data from the test. The black dotted horizontal line specified 50% accuracy level.

In 3D orientation [Figure 5.10], the pair (O3, O4) result from V3d area showed high accuracy and passed the baseline by the lower standard error of the mean with 62.94% prediction accuracy. The area V3v showed high accuracy above the baseline with 60.75% and 59.38% but failed by the lower standard error of the mean. The area V1 and V3a had accuracies in (O3, O4) above the baseline, however, the lower standard error was below the baseline. In other areas, there were around 50% to 57% below each baseline level. The LOC area had the lowest accuracies in 3D orientation.

In 2D orientation [Figure 5.11], the pair (O2, O4) results had high accuracies in V3d, V3v, and KO with 66.13%, 61.50%, and 60.44% respectively. These accuracies surpass the baseline level by the lower standard error of the mean. The same pair results from V1, V2, V3A, LOC, and DIPS had passed the baseline with accuracies of 60.06%, 59.06%, 59.38%, 56.94%, and 57.44% respectively. In other classification pair, the results were just about at the chance level (50%).

Table 5.6 Prediction Accuracy (%) Results from Coarse-precision

ROI	Prediction accuracy (%)					
	3D Orientation		2D Orientation			
	(O1, O2)	(O3, O4)	(O2, O3)	(O1, O3)	(O1, O4)	(O2, O4)
V1	55.69	57.13	48.81	54.06	55.13	60.06
V2	55.25	55.19	49.06	51.88	46.81	59.06
V3d	55.69	**62.94**	55.25	50.19	55.31	**66.13**
V3v	60.75	59.38	52.56	53.31	47.56	**61.50**
V3A	48.50	60.75	47.00	48.38	51.81	59.38
V7	54.56	56.19	55.13	54.94	50.38	56.19
KO	51.69	50.75	48.94	53.63	48.88	**60.44**
hMT+	55.75	49.38	54.13	51.75	53.69	50.56
LOC	47.06	41.00	51.81	47.69	43.69	56.94
VIPS	50.31	50.50	49.19	54.38	41.19	51.44
POIPS	47.13	55.44	51.75	57.00	52.69	46.44
DIPS	50.56	52.63	52.19	52.50	43.44	57.44

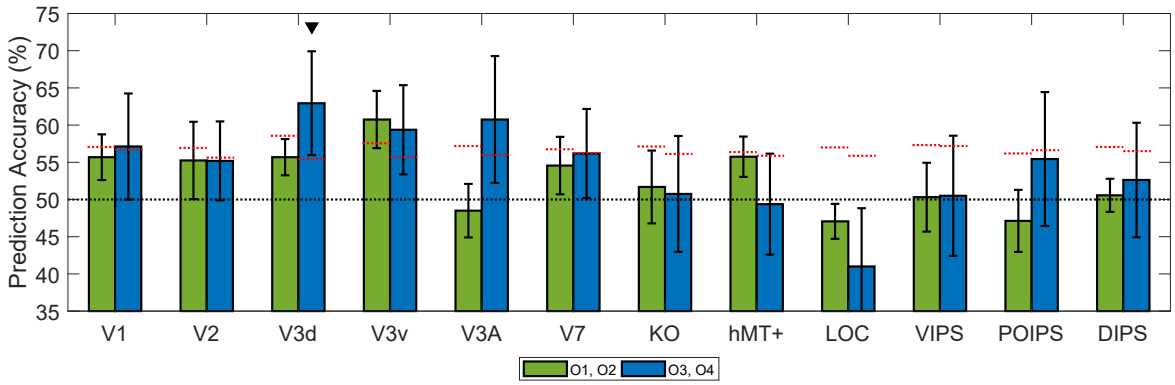

Fig. 5.10 Coarse-precision 3D orientation classification accuracy each ROI

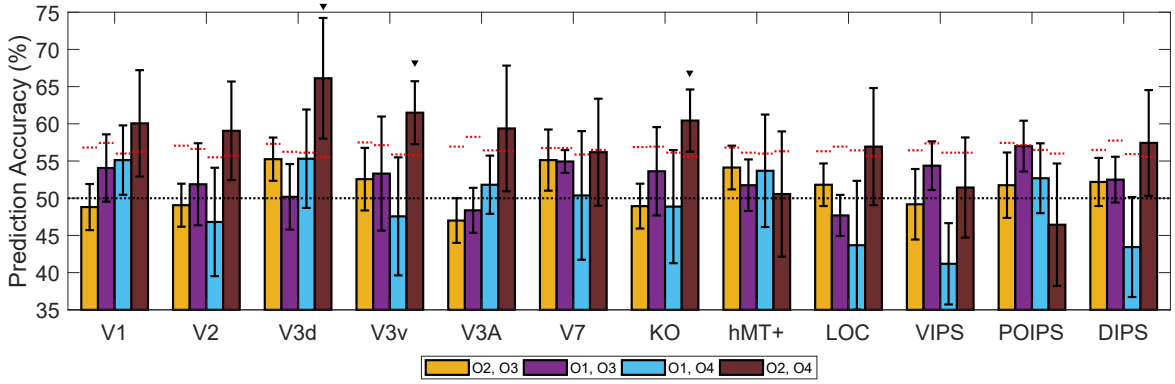

Fig. 5.11 Coarse-precision 2D orientation classification accuracy each ROI

5.3.3 Precision-abstract classification

The precision-abstract classification predictions from all pairs were presented in [Table 5.7] and illustrated in [Figure 5.12] and [Figure 5.13] in bar charts. The error bars in both figures represented the standard error of the mean from each classification. The red dotted horizontal lines marked the chance level baseline generated from permutation test. The lines level indicated upper 99.6% centile of the distribution of permuted data from the test. The black dotted horizontal line specified 50% accuracy level.

In 3D orientation [Figure 5.12], the pair (O1, O2) results from V2 and KO area showed high accuracy passed the baseline with accuracies of 58.50% and 57.63%, but the lower standard error of the mean were below the baseline. The area V3v showed high accuracy above the baseline with 60.75% and 59.38% but failed by the lower standard error of the mean. The area V1 and DIPS had accuracies in (O3, O4) above the baseline, however, the lower standard error was below the baseline. In other areas, the results were varied and all were below each baseline level. V3A and V7 areas had the lowest accuracies in 3D orientation especially in pair (O3, O4).

In 2D orientation [Figure 5.13], the pair (O1, O3) results had high accuracies in V1 with 60.56% above the baseline by the lower standard error of the mean. Some results in V1, V2, and V3d were above the baseline, but the lower standard error of the mean was below the baseline. The rest of the results showed varied accuracies with no significant difference.

Table 5.7 Prediction Accuracy (%) Results from Precision-abstract

ROI	Prediction accuracy (%)					
	3D Orientation		2D Orientation			
	(O1, O2)	(O3, O4)	(O2, O3)	(O1, O3)	(O1, O4)	(O2, O4)
V1	56.19	56.56	55.25	**60.56**	58.50	50.56
V2	58.50	55.06	52.00	60.25	45.56	57.06
V3d	50.31	42.19	50.63	48.06	41.06	57.63
V3v	55.25	53.06	55.06	56.94	43.00	53.13
V3A	45.63	36.31	53.13	47.00	53.44	50.50
V7	46.63	34.88	53.31	49.00	44.56	41.69
KO	57.63	50.19	49.75	55.19	51.19	46.38
hMT+	48.44	47.31	53.06	55.44	53.69	45.06
LOC	48.25	51.31	53.06	52.50	43.94	40.31
VIPS	51.63	44.00	51.06	50.38	45.38	46.69
POIPS	45.19	48.19	52.06	52.06	44.69	46.44
DIPS	46.38	57.25	51.38	49.25	45.44	52.38

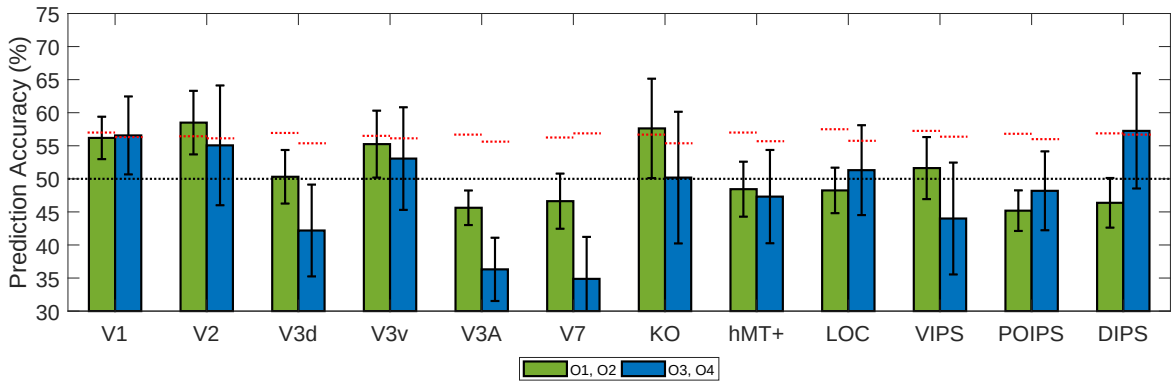

Fig. 5.12 Precision-abstract 3D orientation classification accuracy each ROI

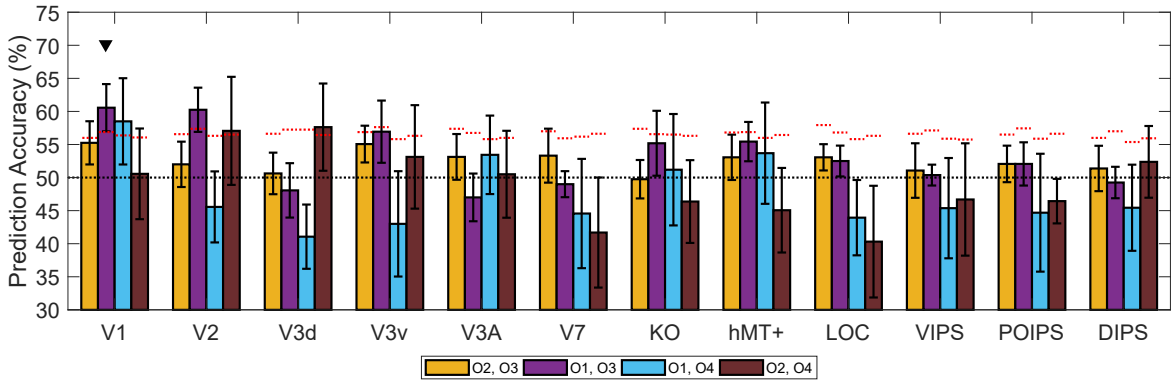

Fig. 5.13 Precision-abstract 2D orientation classification accuracy each ROI

5.4 Generalized stimuli classification

The Generalized stimuli classification predictions from all pairs were presented in table [Table 5.8] and illustrated in [Figure 5.14] and [Figure 5.15] in bar charts. The error bars in both figures represented the standard error of the mean from each classification. The red dotted horizontal lines marked the chance level baseline generated from permutation test. The lines level indicated upper 99.6% centile of the distribution of permuted data from the test. The black dotted horizontal line specified 50% accuracy level.

In the first pair (O1, O2) from 3D orientation classification in the generalized category, the result showed no significant prediction accuracy in all ROIs. In contrast, the pair of (O3, O4) had high accuracies of ROIs in dorsal areas; V7, KO, MT+, VIPS, and DIPS, passed the baseline by each lower standard error of the mean. The top three prediction accuracies were from on KO, VIPS, and V7 area with 60.5%, 59.3%, and 59.1% [Figure 5.14].

In orientation pair from 2D orientation classification [Figure 5.15], the result of the pair (O2, O3) showed high prediction accuracy in V3V that passed the baseline and had the accuracy of 57.8%. The result from (O1, O3) showed high prediction accuracy in KO area (60.7%) and passed the baseline. The other orientation pairs resulted differently. In (O1, O4), the prediction accuracy from LOC and DIPS fell behind the baseline while other areas had high accuracy and passed the baseline. The prediction accuracies from V2, V3V, V7, KO, and POIPS were all above 60%. The result from (O2, O4) had a similar trend with the (O1, O4) pair. The prediction accuracy from V1, V2, V3A, hMT+, and LOC fell behind the baseline while other areas had high accuracy and passed the baseline. The area KO showed the highest accuracy (61.1%).

Table 5.8 Prediction Accuracy (%) Results from Generalized Stimuli

ROI	Prediction accuracy (%)					
	3D Orientation		2D Orientation			
	(O1, O2)	(O3, O4)	(O2, O3)	(O1, O3)	(O1, O4)	(O2, O4)
V1	50.04	53.29	52.13	57.08	**57.33**	54.46
V2	53.50	54.75	55.29	57.42	**62.96**	56.33
V3d	52.79	54.50	51.71	52.29	**57.92**	**59.08**
V3v	49.58	57.42	**57.79**	59.71	**60.29**	**59.25**
V3A	50.63	55.50	51.33	55.54	**56.75**	55.71
V7	53.79	**59.08**	51.38	55.63	**61.96**	**59.58**
KO	51.83	**60.46**	52.29	**60.71**	**66.79**	**61.08**
hMT+	48.00	**57.29**	54.71	51.13	**56.88**	56.88
LOC	47.58	52.46	48.54	46.00	57.63	53.88
VIPS	52.79	**59.33**	51.92	57.88	**64.17**	**59.71**
POIPS	52.75	56.21	50.00	50.42	**59.46**	**56.92**
DIPS	49.67	56.67	49.67	51.79	57.71	**57.92**

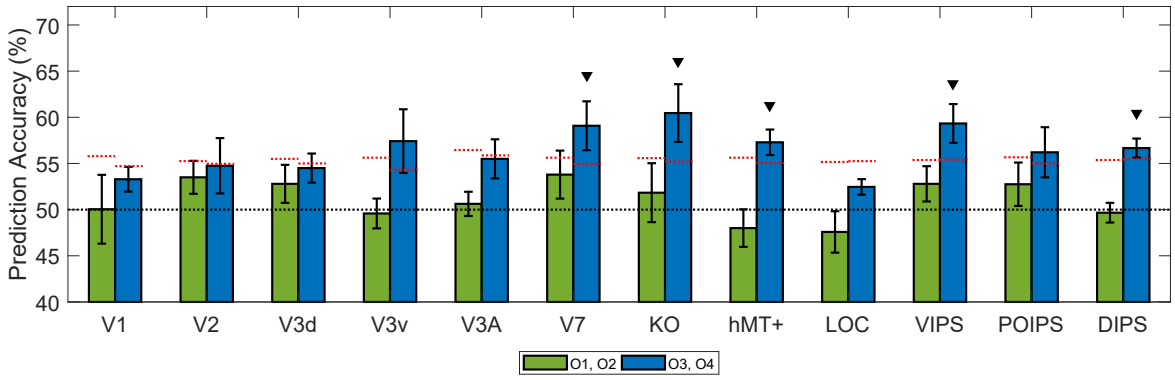

Fig. 5.14 Generalized stimuli 3D orientation classification accuracy each ROI

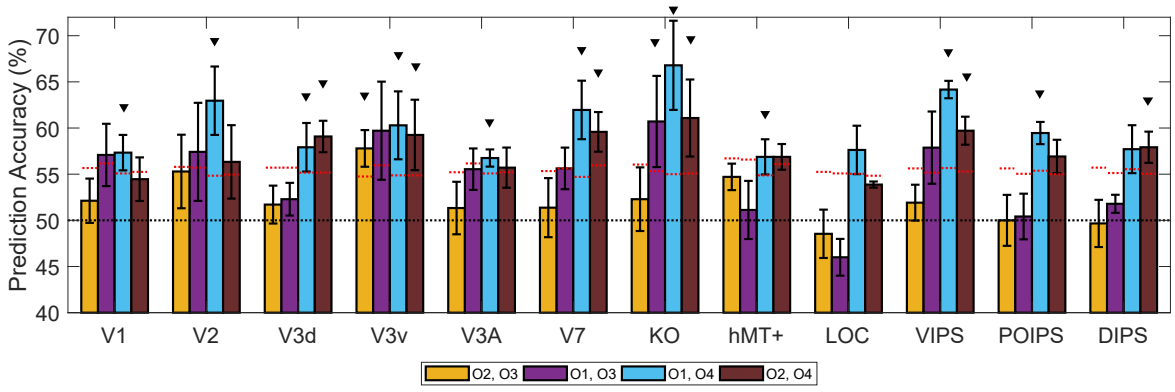

Fig. 5.15 Generalized stimuli 2D orientation classification accuracy each ROI

Chapter 6

Discussion and Conclusion

This chapter represents the insights discussion on the analysis and any tendency discovery from data. The relation between this study analysis and background research is emphasized.

6.1 Discussion

The result from perception performance test had supported that there is no significant difference between the distinct stimuli type of same orientation from all participants. The ANOVA of each orientation did not reject the null hypothesis.

From all same-type classification, the coarse grip type only classification had shown diverge from other one type classifications. Only V1 and KO areas showed high accuracy in some classification pairs whereas other areas failed to pass the chance level baseline by the lower standard error.

However, the result from other two (abstract only and precision only) showed similar trends in 3D orientation classification with significantly high accuracy in dorsal area; KO and VIPS areas. In 2D orientation, the abstract only had significantly high accuracy on V3v area but the precision only had significantly high accuracy on V2, V3A, V7, KO, hMT+, LOC, VIPS, POIPS, and DIPS area. These data suggest that abstract and precision grip stimuli had a tendency for 3D orientation classification.

High contrast in overall prediction accuracies from coarse and precision perhaps

affected by difference process for these two grasp types. Coarse grip object was easy to grasp and there were small changes between the different orientations. On the other hand, precision grip object may process differently in a specific orientation.

Combining the 2D and 3D orientation results of O4 related classification pairs: (O3, O4),(O1, O4), and (O2, O4), there were high prediction accuracies in precision type classification in most ROIs, while other two stimuli types had less tendency showed. This aspect shows the likelihood of a distinct processed in O4 apart from O1, O2, and O3 on precision grip action.

In transfer-type classification, the results mixed and varied around the chance level. The coarse-precision classification had shown a similar characteristic of O4 pairs accuracies with the precision only classification in ROIs from V3d, V3v, and KO in 2D orientation. However, the 3D orientation had no similarities of both. This proposed the possibility of having a different process for precision type in 3D orientation related to action.

Lastly, in the generalized stimuli classification, the result in 3D orientation classification, the (O3, O4) pair had significantly high prediction accuracy from MVPA in dorsal areas; V7, KO, VIPS, and DIPS. On the other hand, in 2D orientation, pairs of (O1, O4) and (O2, O4) showed high prediction accuracy in some early visual areas and dorsal areas as well.

There is an interesting aspect to both 2D and 3D classifications from pairs involving O4 from the same-type and generalized classification. These classifications had high accuracy in KO and IPS areas. The alignment of objects in O4 may relate to the participant's right-hand posture that was holding a controller during the experiment [Figure 6.1]. The effects on the high accuracies of O4 related pairs also showed in the abstract only's 3D orientation classification and precision only's both orientation classifications as well. This suggests that there may be a special process for 3D orientation related to

action and self-body and need to study further for a better explanation.

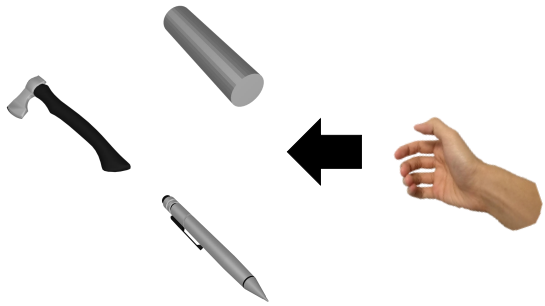

Fig. 6.1 Participants' hand alignment and O4 orientation of 3D object

6.2 Conclusion

This thesis consisted of the introduction of research which construct from background research on two stream hypothesis, the grasping and tools object, and 3D orientation studies. The MVPA classification and permutation were utilized on the fMRI experiment data. Lastly, the result and discussion from the experiment. These topics available in chapter 1 to chapter 6 respectively.

First, the background research was present from past years. The two stream hypothesis was the fundamental theory about the vision to action and vision for perception that many research were branched out several new paths. One branch was the study in the orientation sensitivity of dorsal stream on the graspable object. Human visuomotor system evokes on action planning task (i.e grasping) even when viewing the image of objects. This factor was explored on the features or properties of the objects to find what was evoked the visual for action. The tool's properties of the graspable object were proposed and studied in a great deal. Among the tool-like stimuli used in the experiment, the elongated shape indicated the priming effect of tool-like object. Furthermore, the grasp types with precision on object showed high brain activity on hAIPS inde-

pendently of stimulus size. Other studies also supported these discoveries on elongate shape and ROI in IPS area of dorsal stream has high activity when involving vision to action related task. On the other side, the previous 3D orientation research discovered the IPS and KO area has the tendency for 3D orientation classification.

These research background had given us a general idea and we proposed to investigate the connection of 3D orientation and object that has action related feature. We used MVPA classification and permutation scheme for statistical test the significance of results. In an fMRI experiment design, we applied 3 types of 3D object stimuli (abstract, coarse grip, precision only) with 4 different orientation for each type.

The result from MVPA classification in each ROI presented the significantly high prediction rate on KO and VIPS area in 2D and 3D orientation of abstract object, precision grip, and generalized stimuli. However, the result from coarse grip stimuli showed relatively low accuracy in the KO and VIPS area. The KO and VIPS areas results in 2D orientation classification may be different in each stimuli type but show a similar tendency in 3D orientation classification.

Other interesting finding involved the O4 orientation. The high prediction accuracies were mostly from the classification associated with O4. Our idea to support this phenomenon was that O4 orientation had aligned congruently with participants' hand when holding the controller in the experiment. Another interesting idea was the precision grip object may have a different process for orientation that causes the voxel pattern to be better classified. This may refer that the hand orientation may influence the perception of an object in the compatible orientation. There may be some self-body relation with the stimuli that need a future study for more solid evidence support. In summary, this study suggests a potential approach to investigate 3D orientation feature that relates to action from dorsal area in visual cortex.

Acknowledgement

First and foremost, I would like my utmost gratitude to Professor Hiroaki Shigemasu for kindly accepted me, who have zero background in fMRI research, into his laboratory and guided every step that I took from the start in this research for the past two years. His "vision" in this vision's perception research helped me through any hardship that I face from literature reviews, experiment design, result's analysis and led me to present my study at Asia-Pacific Conference on Vision in 2019. He doesn't mind helping me in a lot of things even though with a busy schedule. I'm sincerely glad that he will accept me in the Ph.D. under his supervision.

I wish to thank Professor Kiyoshi Nakahara and Professor Hiroshi Kadota for valuable comments and suggestion about my research. I would like to thank my lab senior Zhen Li for giving me a lot of useful advice and taught me the know-how of the fMRI research and helped in everyday life at KUT.

Sincerely thank for all teachers, faculty staff, and IRC staff for every support when I needed. Thank you all friends from Shigematsu lab, KUT campus, and the international house for spending time with me.

I wholeheartedly thank all Thai at KUT friends for beautiful pleasant memories that we shared, all the nostalgic Thai meal that we had together, all the trips that we went. They are proved for our everlasting friendship.

Finally, I have deeply appreciated the support of my family, relatives, and friends from Thailand. They are patiently waiting and giving all the support they can for me. The last person I want to give my gratitude to is my special one who always gives me encouragement whenever I lost my way. Thank you.

References

[1] Goodale, M. A., & Milner, A. D. (1992). Separate visual pathways for perception and action. Trends in Neurosciences, 15(1), 20–25.

[2] Haxby, J. V. (2001). Distributed and Overlapping Representations of Faces and Objects in Ventral Temporal Cortex. Science, 293(5539), 2425–2430.

[3] Norman, K. A., Polyn, S. M., Detre, G. J., & Haxby, J. V. (2006). Beyond mind-reading: multi-voxel pattern analysis of fMRI data. Trends in Cognitive Sciences, 10(9), 424–430.

[4] Valyear, K. F., Culham, J. C., Sharif, N., Westwood, D., & Goodale, M. A. (2006). A double dissociation between sensitivity to changes in object identity and object orientation in the ventral and dorsal visual streams: A human fMRI study. Neuropsychologia, 44(2), 218–228.

[5] Symes, E., Ellis, R., & Tucker, M. (2007). Visual object affordances: Object orientation. Acta Psychologica, 124(2), 238–255.

[6] Rice, N. J., Valyear, K. F., Goodale, M. A., Milner, A. D., & Culham, J. C. (2007). Orientation sensitivity to graspable objects: An fMRI adaptation study. NeuroImage, 36, T87–T93.

[7] Begliomini, C., Caria, A., Grodd, W., & Castiello, U. (2007). Comparing Natural and Constrained Movements: New Insights into the Visuomotor Control of Grasping. PLoS ONE, 2(10), e1108.

[8] Valyear, K. F., Cavina-Pratesi, C., Stiglick, A. J., & Culham, J. C. (2007). Does tool-related fMRI activity within the intraparietal sulcus reflect the plan to grasp? NeuroImage, 36, T94–T108.

[9] Harris, I. M., Benito, C. T., Ruzzoli, M., & Miniussi, C. (2008). Effects of Right

Parietal Transcranial Magnetic Stimulation on Object Identification and Orientation Judgments. Journal of Cognitive Neuroscience, 20(5), 916–926.

[10] Sakuraba, S., Sakai, S., Yamanaka, M., Yokosawa, K., & Hirayama, K. (2012). Does the Human Dorsal Stream Really Process a Category for Tools? Journal of Neuroscience, 32(11), 3949–3953.

[11] Freud, E., Ganel, T., Shelef, I., Hammer, M. D., Avidan, G., & Behrmann, M. (2015). Three-Dimensional Representations of Objects in Dorsal Cortex are Dissociable from Those in Ventral Cortex. Cerebral Cortex, 27(1), 422–434.

[12] Haxby, J. V. (2012). Multivariate pattern analysis of fMRI: The early beginnings. NeuroImage, 62(2), 852–855.

[13] Di Bono, M. G., Begliomini, C., Castiello, U., & Zorzi, M. (2015). Probing the reaching-grasping network in humans through multivoxel pattern decoding. Brain and Behavior, 5(11), e00412.

[14] Murphy, A., Ban, H. and Welchman, A. (2013). Integration of texture and disparity cues to surface slant in dorsal visual cortex. Journal of Neurophysiology, 110(1), pp.190-203.

[15] Dövencioğlu, D., Ban, H., Schofield, A. J., & Welchman, A. E. (2013). Perceptual Integration for Qualitatively Different 3-D Cues in the Human Brain. Journal of Cognitive Neuroscience, 25(9), 1527–1541.

[16] Rosenberg, A., Cowan, N. and Angelaki, D. (2013). The Visual Representation of 3D Object Orientation in Parietal Cortex. Journal of Neuroscience, 33(49), pp.19352-19361.

[17] LIANG, K.-Y., & ZEGER, S. L. (1986). Longitudinal data analysis using generalized linear models. Biometrika, 73(1), 13–22.

[18] Macdonald, S. N., & Culham, J. C. (2015). Do human brain areas involved in visuomotor actions show a preference for real tools over visually similar non-tools?

Neuropsychologia, 77, 35–41.

[19] Orban, G., Claeys, K., Nelissen, K., Smans, R., Sunaert, S., Todd, J., Wardak, C., Durand, J. and Vanduffel, W. (2006). Mapping the parietal cortex of human and non-human primates. Neuropsychologia, 44(13), pp.2647-2667.

[20] Fabbri, S., Stubbs, K. M., Cusack, R., & Culham, J. C. (2016). Disentangling Representations of Object and Grasp Properties in the Human Brain. Journal of Neuroscience, 36(29), 7648–7662.

[21] Etzel, J. A., & Braver, T. S. (2013). MVPA Permutation Schemes: Permutation Testing in the Land of Cross-Validation. In 2013 International Workshop on Pattern Recognition in Neuroimaging. IEEE.

[22] Etzel, J. A. (2015). MVPA Permutation Schemes: Permutation Testing for the Group Level. In 2015 International Workshop on Pattern Recognition in NeuroImaging. IEEE.

[23] Li, Z. and Shigemasu, H. (2018). Generalized representation of stereoscopic surface in V3A. Journal of Vision, 18(10), p.120.

[24] Li, Z. and Shigemasu, H. (2019). Generalized Representation of Stereoscopic Surface Shape and Orientation in the Human Visual Cortex. Frontiers in Human Neuroscience, 13.

[25] Henderson, M., & Serences, J. T. (2019). Human frontoparietal cortex represents behaviorally relevant target status based on abstract object features. Journal of Neurophysiology, 121(4), 1410–1427.

Appendix A

Individual Results

Table A.1 Participant 1 Prediction Accuracy (%) Results from Abstract Only

ROI	Prediction accuracy (%)					
	3D Orientation		2D Orientation			
	(O1, O2)	(O3, O4)	(O2, O3)	(O1, O3)	(O1, O4)	(O2, O4)
V1	65.00	70.00	35.00	57.50	47.50	60.00
V2	57.50	57.50	60.00	57.50	42.50	47.50
V3D	37.50	67.50	40.00	40.00	52.50	45.00
V3V	52.50	57.50	65.00	60.00	57.50	50.00
V3A	45.00	60.00	57.50	42.50	62.50	67.50
V7	57.50	50.00	52.50	57.50	62.50	52.50
KO	75.00	72.50	77.50	60.00	55.00	77.50
MT+	37.50	42.50	45.00	40.00	27.50	45.00
LOC	52.50	62.50	62.50	42.50	40.00	37.50
VIPS	50.00	70.00	62.50	65.00	50.00	62.50
POIPS	52.50	52.50	42.50	55.00	62.50	37.50
DIPS	70.00	40.00	40.00	45.00	50.00	62.50

Table A.2 Participant 2 Prediction Accuracy (%) Results from Abstract Only

ROI	Prediction accuracy (%)					
	3D Orientation		2D Orientation			
	(O1, O2)	(O3, O4)	(O2, O3)	(O1, O3)	(O1, O4)	(O2, O4)
V1	52.50	62.50	67.50	55.00	60.00	65.00
V2	50.00	52.50	57.50	60.00	60.00	70.00
V3D	57.50	52.50	47.50	50.00	55.00	67.50
V3V	75.00	55.00	52.50	80.00	47.50	67.50
V3A	55.00	50.00	50.00	57.50	47.50	60.00
V7	57.50	75.00	42.50	55.00	52.50	50.00
KO	65.00	50.00	55.00	45.00	57.50	62.50
MT+	37.50	55.00	45.00	42.50	50.00	42.50
LOC	35.00	40.00	47.50	27.50	47.50	35.00
VIPS	50.00	65.00	47.50	35.00	45.00	50.00
POIPS	35.00	52.50	42.50	42.50	42.50	60.00
DIPS	32.50	62.50	27.50	45.00	40.00	42.50

Table A.3 Participant 3 Prediction Accuracy (%) Results from Abstract Only

ROI	Prediction accuracy (%)					
	3D Orientation		2D Orientation			
	(O1, O2)	(O3, O4)	(O2, O3)	(O1, O3)	(O1, O4)	(O2, O4)
V1	50.00	43.75	68.75	62.50	40.63	62.50
V2	46.88	50.00	65.63	53.13	43.75	56.25
V3D	46.88	50.00	37.50	59.38	37.50	37.50
V3V	34.38	53.13	59.38	56.25	40.63	65.63
V3A	53.13	62.50	50.00	71.88	53.13	53.13
V7	65.63	43.75	43.75	56.25	62.50	43.75
KO	50.00	56.25	43.75	62.50	50.00	50.00
MT+	59.38	50.00	50.00	56.25	53.13	68.75
LOC	40.63	56.25	46.88	43.75	46.88	62.50
VIPS	50.00	59.38	68.75	53.13	59.38	68.75
POIPS	50.00	43.75	40.63	50.00	50.00	56.25
DIPS	40.63	37.50	43.75	40.63	31.25	40.63

Table A.4 Participant 4 Prediction Accuracy (%) Results from Abstract Only

ROI	Prediction accuracy (%)					
	3D Orientation		2D Orientation			
	(O1, O2)	(O3, O4)	(O2, O3)	(O1, O3)	(O1, O4)	(O2, O4)
V1	55.00	32.50	42.50	52.50	62.50	55.00
V2	47.50	85.00	52.50	57.50	65.00	72.50
V3D	47.50	47.50	67.50	45.00	42.50	47.50
V3V	62.50	72.50	47.50	40.00	57.50	77.50
V3A	47.50	62.50	50.00	52.50	57.50	65.00
V7	45.00	75.00	45.00	62.50	77.50	60.00
KO	47.50	75.00	57.50	47.50	62.50	47.50
MT+	47.50	62.50	65.00	65.00	55.00	67.50
LOC	30.00	50.00	47.50	57.50	47.50	45.00
VIPS	42.50	67.50	57.50	62.50	65.00	60.00
POIPS	42.50	65.00	52.50	70.00	77.50	70.00
DIPS	40.00	55.00	47.50	60.00	60.00	65.00

Table A.5 Participant 5 Prediction Accuracy (%) Results from Abstract Only

ROI	Prediction accuracy (%)					
	3D Orientation		2D Orientation			
	(O1, O2)	(O3, O4)	(O2, O3)	(O1, O3)	(O1, O4)	(O2, O4)
V1	85.00	77.50	52.50	75.00	70.00	67.50
V2	70.00	82.50	57.50	87.50	50.00	70.00
V3D	70.00	67.50	55.00	65.00	42.50	70.00
V3V	60.00	75.00	45.00	70.00	45.00	67.50
V3A	50.00	65.00	55.00	35.00	37.50	60.00
V7	50.00	67.50	57.50	75.00	47.50	52.50
KO	75.00	72.50	45.00	80.00	47.50	70.00
MT+	65.00	72.50	65.00	67.50	75.00	75.00
LOC	42.50	52.50	45.00	65.00	67.50	70.00
VIPS	50.00	57.50	55.00	65.00	45.00	57.50
POIPS	62.50	67.50	67.50	35.00	60.00	52.50
DIPS	65.00	65.00	52.50	62.50	70.00	45.00

Table A.6 Participant 1 Prediction Accuracy (%) Results from Coarse Only

ROI	Prediction accuracy (%)					
	3D Orientation		2D Orientation			
	(O1, O2)	(O3, O4)	(O2, O3)	(O1, O3)	(O1, O4)	(O2, O4)
V1	57.50	60.00	75.00	50.00	45.00	72.50
V2	62.50	60.00	67.50	60.00	60.00	72.50
V3D	55.00	47.50	62.50	52.50	60.00	65.00
V3V	47.50	42.50	57.50	55.00	40.00	52.50
V3A	42.50	57.50	65.00	40.00	35.00	50.00
V7	57.50	45.00	65.00	55.00	45.00	55.00
KO	50.00	52.50	65.00	50.00	45.00	52.50
MT+	35.00	50.00	40.00	47.50	57.50	40.00
LOC	50.00	50.00	55.00	37.50	52.50	55.00
VIPS	50.00	27.50	60.00	57.50	60.00	57.50
POIPS	50.00	57.50	47.50	30.00	50.00	50.00
DIPS	37.50	52.50	40.00	32.50	37.50	52.50

Table A.7 Participant 2 Prediction Accuracy (%) Results from Coarse Only

ROI	Prediction accuracy (%)					
	3D Orientation		2D Orientation			
	(O1, O2)	(O3, O4)	(O2, O3)	(O1, O3)	(O1, O4)	(O2, O4)
V1	52.50	52.50	62.50	50.00	40.00	52.50
V2	35.00	47.50	57.50	57.50	55.00	57.50
V3D	50.00	57.50	45.00	52.50	60.00	47.50
V3V	57.50	62.50	62.50	70.00	57.50	77.50
V3A	47.50	62.50	42.50	50.00	55.00	40.00
V7	40.00	60.00	57.50	67.50	45.00	40.00
KO	42.50	65.00	57.50	52.50	55.00	65.00
MT+	60.00	42.50	62.50	50.00	52.50	62.50
LOC	37.50	50.00	57.50	52.50	45.00	45.00
VIPS	35.00	65.00	52.50	62.50	60.00	65.00
POIPS	47.50	57.50	70.00	60.00	50.00	70.00
DIPS	55.00	52.50	45.00	55.00	60.00	35.00

Table A.8 Participant 3 Prediction Accuracy (%) Results from Coarse Only

ROI	Prediction accuracy (%)					
	3D Orientation		2D Orientation			
	(O1, O2)	(O3, O4)	(O2, O3)	(O1, O3)	(O1, O4)	(O2, O4)
V1	62.50	62.50	71.88	50.00	75.00	78.13
V2	53.13	56.25	46.88	62.50	65.63	50.00
V3D	59.38	46.88	43.75	62.50	56.25	43.75
V3V	37.50	53.13	65.63	37.50	65.63	28.13
V3A	78.13	62.50	59.38	68.75	59.38	71.88
V7	68.75	56.25	50.00	53.13	62.50	46.88
KO	59.38	62.50	43.75	37.50	40.63	62.50
MT+	56.25	75.00	40.63	46.88	25.00	50.00
LOC	59.38	37.50	53.13	68.75	59.38	62.50
VIPS	50.00	59.38	56.25	37.50	37.50	50.00
POIPS	43.75	53.13	34.38	43.75	50.00	43.75
DIPS	50.00	50.00	25.00	53.13	37.50	40.63

Table A.9 Participant 4 Prediction Accuracy (%) Results from Coarse Only

ROI	Prediction accuracy (%)					
	3D Orientation		2D Orientation			
	(O1, O2)	(O3, O4)	(O2, O3)	(O1, O3)	(O1, O4)	(O2, O4)
V1	72.50	50.00	57.50	57.50	45.00	50.00
V2	65.00	60.00	47.50	60.00	60.00	60.00
V3D	60.00	65.00	47.50	65.00	50.00	65.00
V3V	70.00	72.50	50.00	42.50	60.00	72.50
V3A	55.00	45.00	40.00	72.50	77.50	52.50
V7	55.00	65.00	47.50	52.50	55.00	57.50
KO	55.00	40.00	62.50	52.50	35.00	52.50
MT+	60.00	50.00	45.00	57.50	45.00	52.50
LOC	45.00	45.00	37.50	27.50	50.00	57.50
VIPS	62.50	35.00	52.50	65.00	60.00	55.00
POIPS	50.00	45.00	45.00	62.50	50.00	50.00
DIPS	62.50	47.50	47.50	37.50	62.50	45.00

Table A.10 Participant 5 Prediction Accuracy (%) Results from Coarse Only

ROI	Prediction accuracy (%)					
	3D Orientation		2D Orientation			
	(O1, O2)	(O3, O4)	(O2, O3)	(O1, O3)	(O1, O4)	(O2, O4)
V1	67.50	70.00	60.00	75.00	67.50	55.00
V2	75.00	85.00	45.00	85.00	60.00	75.00
V3D	65.00	52.50	60.00	72.50	57.50	67.50
V3V	77.50	65.00	32.50	80.00	57.50	65.00
V3A	45.00	50.00	42.50	30.00	50.00	62.50
V7	62.50	52.50	45.00	77.50	55.00	55.00
KO	85.00	82.50	60.00	77.50	67.50	85.00
MT+	70.00	50.00	70.00	40.00	35.00	40.00
LOC	62.50	50.00	45.00	50.00	65.00	42.50
VIPS	67.50	57.50	60.00	55.00	52.50	45.00
POIPS	40.00	52.50	37.50	65.00	55.00	55.00
DIPS	32.50	45.00	45.00	50.00	52.50	50.00

Table A.11 Participant 1 Prediction Accuracy (%) Results from Precision Only

ROI	Prediction accuracy (%)					
	3D Orientation		2D Orientation			
	(O1, O2)	(O3, O4)	(O2, O3)	(O1, O3)	(O1, O4)	(O2, O4)
V1	62.50	50.00	67.50	52.50	65.00	57.50
V2	62.50	50.00	62.50	45.00	70.00	62.50
V3D	75.00	52.50	55.00	55.00	62.50	55.00
V3V	62.50	50.00	40.00	40.00	57.50	52.50
V3A	72.50	52.50	55.00	52.50	65.00	55.00
V7	45.00	62.50	65.00	42.50	57.50	65.00
KO	60.00	62.50	62.50	50.00	62.50	65.00
MT+	35.00	60.00	47.50	42.50	57.50	60.00
LOC	60.00	60.00	50.00	50.00	67.50	60.00
VIPS	47.50	65.00	25.00	35.00	52.50	62.50
POIPS	50.00	62.50	50.00	37.50	67.50	60.00
DIPS	42.50	55.00	42.50	42.50	60.00	67.50

Table A.12 Participant 2 Prediction Accuracy (%) Results from Precision Only

ROI	Prediction accuracy (%)					
	3D Orientation		2D Orientation			
	(O1, O2)	(O3, O4)	(O2, O3)	(O1, O3)	(O1, O4)	(O2, O4)
V1	37.50	62.50	47.50	35.00	65.00	57.50
V2	50.00	65.00	45.00	47.50	62.50	65.00
V3D	50.00	60.00	55.00	60.00	62.50	65.00
V3V	72.50	62.50	47.50	75.00	70.00	65.00
V3A	52.50	60.00	47.50	37.50	52.50	57.50
V7	25.00	60.00	60.00	57.50	55.00	55.00
KO	55.00	67.50	62.50	42.50	55.00	67.50
MT+	40.00	50.00	55.00	40.00	60.00	72.50
LOC	42.50	57.50	52.50	40.00	70.00	72.50
VIPS	37.50	65.00	40.00	55.00	55.00	65.00
POIPS	32.50	62.50	52.50	50.00	60.00	60.00
DIPS	45.00	60.00	65.00	65.00	60.00	62.50

Table A.13 Participant 3 Prediction Accuracy (%) Results from Precision Only

ROI	Prediction accuracy (%)					
	3D Orientation		2D Orientation			
	(O1, O2)	(O3, O4)	(O2, O3)	(O1, O3)	(O1, O4)	(O2, O4)
V1	68.75	56.25	62.50	37.50	53.13	50.00
V2	43.75	68.75	53.13	46.88	53.13	50.00
V3D	53.13	56.25	46.88	34.38	62.50	53.13
V3V	56.25	53.13	75.00	53.13	53.13	59.38
V3A	43.75	78.13	31.25	50.00	59.38	68.75
V7	43.75	87.50	59.38	50.00	75.00	68.75
KO	34.38	78.13	46.88	46.88	62.50	62.50
MT+	46.88	78.13	53.13	59.38	59.38	56.25
LOC	37.50	50.00	40.63	31.25	56.25	53.13
VIPS	53.13	90.63	78.13	50.00	65.63	62.50
POIPS	62.50	81.25	59.38	46.88	56.25	65.63
DIPS	53.13	84.38	68.75	43.75	59.38	65.63

Table A.14 Participant 4 Prediction Accuracy (%) Results from Precision Only

ROI	Prediction accuracy (%)					
	3D Orientation		2D Orientation			
	(O1, O2)	(O3, O4)	(O2, O3)	(O1, O3)	(O1, O4)	(O2, O4)
V1	35.00	52.50	60.00	37.50	50.00	52.50
V2	47.50	55.00	57.50	42.50	57.50	55.00
V3D	70.00	57.50	47.50	42.50	52.50	62.50
V3V	45.00	57.50	40.00	52.50	60.00	55.00
V3A	55.00	57.50	35.00	42.50	60.00	60.00
V7	47.50	57.50	42.50	42.50	57.50	57.50
KO	65.00	62.50	45.00	52.50	70.00	70.00
MT+	47.50	60.00	42.50	65.00	55.00	57.50
LOC	50.00	57.50	25.00	62.50	67.50	57.50
VIPS	47.50	62.50	32.50	65.00	62.50	60.00
POIPS	47.50	55.00	50.00	45.00	62.50	60.00
DIPS	40.00	70.00	50.00	42.50	65.00	62.50

Table A.15 Participant 5 Prediction Accuracy (%) Results from Precision Only

ROI	Prediction accuracy (%)					
	3D Orientation		2D Orientation			
	(O1, O2)	(O3, O4)	(O2, O3)	(O1, O3)	(O1, O4)	(O2, O4)
V1	50.00	67.50	47.50	67.50	55.00	65.00
V2	75.00	75.00	52.50	85.00	67.50	80.00
V3D	80.00	80.00	35.00	45.00	85.00	95.00
V3V	57.50	70.00	50.00	62.50	75.00	77.50
V3A	62.50	75.00	50.00	42.50	80.00	80.00
V7	82.50	72.50	42.50	47.50	77.50	85.00
KO	82.50	82.50	55.00	75.00	85.00	90.00
MT+	62.50	72.50	42.50	40.00	60.00	77.50
LOC	52.50	80.00	57.50	42.50	62.50	75.00
VIPS	60.00	67.50	47.50	57.50	57.50	70.00
POIPS	47.50	72.50	55.00	55.00	60.00	77.50
DIPS	42.50	65.00	50.00	55.00	55.00	60.00

Table A.16 Participant 1 Prediction Accuracy (%) Results from Generalized stimuli

ROI	Prediction accuracy (%)					
	3D Orientation		2D Orientation			
	(O1, O2)	(O3, O4)	(O2, O3)	(O1, O3)	(O1, O4)	(O2, O4)
V1	40.00	53.33	56.67	52.50	50.83	57.50
V2	55.83	54.17	60.00	45.83	56.67	55.00
V3D	50.83	50.83	55.83	47.50	59.17	54.17
V3V	45.00	52.50	61.67	46.67	48.33	52.50
V3A	45.83	55.83	49.17	50.00	55.83	50.00
V7	63.33	65.83	65.00	53.33	57.50	62.50
KO	60.83	63.33	55.83	63.33	61.67	55.00
MT+	44.17	51.67	50.83	44.17	58.33	52.50
LOC	51.67	54.17	55.83	46.67	62.50	53.33
VIPS	49.17	65.00	55.00	69.17	61.67	62.50
POIPS	45.00	60.00	44.17	40.83	59.17	50.83
DIPS	50.00	56.67	43.33	53.33	54.17	56.67

Table A.17 Participant 2 Prediction Accuracy (%) Results from Generalized stimuli

ROI	Prediction accuracy (%)					
	3D Orientation		2D Orientation			
	(O1, O2)	(O3, O4)	(O2, O3)	(O1, O3)	(O1, O4)	(O2, O4)
V1	40.00	58.33	44.17	47.50	57.50	50.83
V2	47.50	58.33	45.83	51.67	57.50	59.17
V3D	60.00	56.67	43.33	55.00	57.50	60.00
V3V	49.17	70.83	61.67	80.00	69.17	66.67
V3A	52.50	62.50	42.50	53.33	55.83	60.83
V7	56.67	62.50	45.00	53.33	54.17	65.00
KO	48.33	64.17	46.67	53.33	60.00	60.83
MT+	43.33	60.83	53.33	48.33	54.17	55.83
LOC	49.17	51.67	44.17	37.50	58.33	53.33
VIPS	59.17	60.83	46.67	57.50	65.83	53.33
POIPS	53.33	55.00	45.00	55.00	55.83	62.50
DIPS	52.50	60.00	51.67	50.00	60.83	63.33

Table A.18 Participant 3 Prediction Accuracy (%) Results from Generalized stimuli

ROI	Prediction accuracy (%)					
	3D Orientation		2D Orientation			
	(O1, O2)	(O3, O4)	(O2, O3)	(O1, O3)	(O1, O4)	(O2, O4)
V1	59.38	48.96	48.96	56.25	58.33	48.96
V2	50.00	43.75	44.79	52.08	61.46	45.83
V3D	53.13	54.17	51.04	48.96	56.25	60.42
V3V	52.08	47.92	53.13	59.38	57.29	47.92
V3A	48.96	58.33	54.17	59.38	56.25	55.21
V7	53.13	60.42	46.88	48.96	61.46	60.42
KO	45.83	48.96	40.63	59.38	61.46	47.92
MT+	50.00	57.29	59.38	44.79	63.54	55.21
LOC	52.08	53.13	55.21	50.00	48.96	55.21
VIPS	48.96	62.50	47.92	51.04	66.67	59.38
POIPS	56.25	51.04	45.83	56.25	61.46	56.25
DIPS	45.83	58.33	58.33	48.96	67.71	56.25

Table A.19 Participant 4 Prediction Accuracy (%) Results from Generalized stimuli

ROI	Prediction accuracy (%)					
	3D Orientation		2D Orientation			
	(O1, O2)	(O3, O4)	(O2, O3)	(O1, O3)	(O1, O4)	(O2, O4)
V1	55.00	52.50	51.67	59.17	55.83	51.67
V2	57.50	53.33	57.50	57.50	60.00	50.00
V3D	45.83	60.00	55.83	51.67	49.17	55.83
V3V	46.67	59.17	51.67	49.17	56.67	58.33
V3A	54.17	51.67	49.17	63.33	55.00	50.83
V7	48.33	48.33	48.33	59.17	61.67	50.83
KO	44.17	56.67	55.83	47.50	62.50	66.67
MT+	55.83	57.50	52.50	62.50	50.83	60.83
LOC	46.67	49.17	45.83	46.67	53.33	53.33
VIPS	56.67	56.67	51.67	45.83	61.67	60.83
POIPS	60.00	65.83	56.67	51.67	63.33	60.00
DIPS	51.67	54.17	51.67	55.00	53.33	52.50

Table A.20 Participant 5 Prediction Accuracy (%) Results from Generalized stimuli

ROI	Prediction accuracy (%)					
	3D Orientation		2D Orientation			
	(O1, O2)	(O3, O4)	(O2, O3)	(O1, O3)	(O1, O4)	(O2, O4)
V1	55.83	53.33	59.17	70.00	64.17	63.33
V2	56.67	64.17	68.33	80.00	79.17	71.67
V3D	54.17	50.83	52.50	58.33	67.50	65.00
V3V	55.00	56.67	60.83	63.33	70.00	70.83
V3A	51.67	49.17	61.67	51.67	60.83	61.67
V7	47.50	58.33	51.67	63.33	75.00	59.17
KO	60.00	69.17	62.50	80.00	88.33	75.00
MT+	46.67	59.17	57.50	55.83	57.50	60.00
LOC	38.33	54.17	41.67	49.17	65.00	54.17
VIPS	50.00	51.67	58.33	65.83	65.00	62.50
POIPS	49.17	49.17	58.33	48.33	57.50	55.00
DIPS	48.33	54.17	43.33	51.67	52.50	60.83